Electronic Supplementary Material (ESI) for Dalton Transactions.

Supporting Information

Synthesis and anti-microbial activity of a new series of bis(diphosphine) rhenium(V) dioxo complexes

Saul M. Cooper,[a] Christina Siakalli,[a] Andrew J. P. White,[a] Angelo Frei,[a] Philip W. Miller,[a]* Nicholas J. Long[a]*

a) Department of Chemistry, Imperial College London, Molecular Sciences Research Hub, 82 Wood Lane, White City Campus, London, W12 0BZ, UK

*Corresponding Authors: Nicholas J. Long (n.long@imperial.ac.uk)

Philip W. Miller (philip.miller@imperial.ac.uk)

S1) General Materials and Methods

Materials. Ligand syntheses were performed under an N_2 atmosphere using standard Schlenk techniques, unless otherwise stated. Subsequent syntheses of complexes were performed in air. Dry solvents were obtained from an MBraun MB-SPS 800 Solvent Purification system, degassed by thoroughly sparging with nitrogen and stored over activated 3 Å molecular sieves.

$[Ph_2P(CH_2OH)_2]Cl$,[1] $NP_2^{Ph}OH^{Ar,}$,[2] $NP_2^{Ph}COOH^{Me}$,[3] $NP_2^{Ph}COOH^{Bn}$,[2] $NP_2^{Ph}Me$,[4] $NP_2^{Ph}iPr$,[5] $NP_2^{Ph}tBu$,[4] $NP_2^{Ph}Cyh$,[6] and $NP_2^{Ph}Bn$[7] were all prepared as described in the literature. Other reagents were commercially available and were used as received.

Physical Measurements. ^{1}H, $^{31}P\{^{1}H\}$, and $^{13}C\{^{1}H\}$ NMR spectra were recorded on a Bruker AV-400 spectrometer. Chemical shifts are reported in ppm, using the residual proton impurities in the solvents for ^{1}H and $^{13}C\{^{1}H\}$ NMR spectroscopy. ^{31}P chemical shifts were referenced (δ = 0) externally to 85% $H_3PO_{4(aq)}$. Peak multiplicities are abbreviated as; s = singlet, m = multiplet, d = doublet, t = triplet, q = quartet, qu = quintet, sx = sextet, spt = septet, dd = doublet of doublet, td = triplet of doublet, and br = broad. Mass spectrometry analyses were conducted by the Mass Spectrometry Service, Imperial College London. Infrared spectra were recorded on a PerkinElmer Spectrum FT-IR spectrometer.

Flash silica column chromatography was performed on a Biotage Isolera Prime advanced automated flash purification unit using 10g, 25g or 50g SNAP KP-Sil or Sfar Duo cartridges, unless otherwise stated. X-ray diffraction analysis was carried out by Dr Andrew White of the Department of Chemistry at Imperial College London. Details of the single crystal X-ray diffraction analysis can be found in Section S5.

S2) Synthetic Procedures

General procedure for the synthesis of $NP_2^{Ph}X^R$ ligands and $[ReO_2(NP_2^{Ph}X^R)_2]I$ complexes

A Schlenk flask was charged with paraformaldehyde (0.32 g, 10.6 mmol), and diphenylphosphine (1.86 mL, 10.6 mmol) was added under N_2. The reaction mixture was heated to 110 °C for 3 h after which time a translucent, viscous liquid was formed. The liquid was cooled to 60 °C and MeOH (20 mL) added to the flask. The selected primary amine (5.3 mmol, 0.5 eq) was added via syringe and the reaction mixture heated at 60 °C for 18 h. An aliquot (600 µL) was taken for analysis to confirm conversion (> 90 % by $^{31}P\{^1H\}$ NMR) to the $NP_2^{Ph}X^R$ ligand. The volatiles were removed *in vacuo* and the sticky residue re-dissolved in minimal CH_2Cl_2. Upon addition of hexane (50 mL) and vigorous stirring for 10 min, an off-white precipitate was formed and the supernatant removed by filtration. Further hexane washes (2 x 50 mL) yielded the product as an off-white solid. In the case of ligands which did not form a fine powder, following hexane washes the residue was re-dissolved in MeOH (10 mL) and stored under N_2 at – 10 °C. $[ReO_2I(PPh_3)_2]$ (50 mg, 0.057 mmol) was dissolved in CH_2Cl_2 (10 mL). The $NP_2^{Ph}X^R$ ligand (0.13 mmol, 2.2 eq) was added and the reaction mixture stirred at RT for 16 h. Over this period, the solution underwent a colour change from violet to orange to yellow. If a precipitate was formed, this was collected by filtration, washed with hexane (3 x 10 mL), and dried under vacuum. If no precipitate was formed, the solvent was removed *in vacuo*, the residue redissolved in minimal CH_2Cl_2 and precipitated with hexane. This was repeated three times. After isolation by filtration, the crude mixture was purified by silica column chromatography (95:5 $\Rightarrow$ 90:10 v:v CH_2Cl_2:MeOH) to give the product as an off-white solid.

Alternative synthetic procedure using $[Ph_2P(CH_2OH)_2]Cl$

A Schlenk flask was charged with $[Ph_2P(CH_2OH)_2]Cl$ (0.51 g, 1.97 mmol) and dissolved in MeOH (10 mL). DIPEA (0.31 mL, 1.79 mmol) was added via syringe. The primary amine (0.90 mmol) was added via syringe and the reaction mixture heated to 60 °C for 18 h. An aliquot (600 µL) was taken for $^{31}P\{^1H\}$ NMR analysis to confirm conversion to the $NP_2^{Ph}X^R$ ligand. The flask was stored under N_2 at – 10 °C for further use. This ligand solution contained an [DIPEA.H]Cl byproduct which could be removed upon purification of the complex by silica column chromatography.

Isolated yields are reported which respect to the *complex formation* using either the isolated ligand or stock solution.

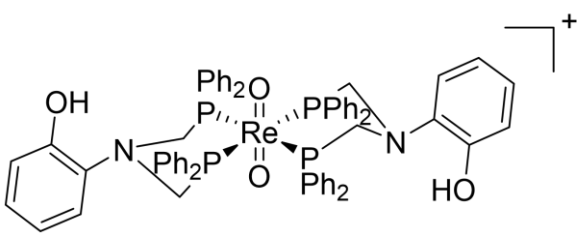

I^- *[ReO₂(κ²-NP₂^PhOH^Ar)₂]I* (**ReO₂-NP₂OH**) (**Re-1**): 86%. ^{1}H NMR (400 MHz, d^3-MeOD): δ_H /ppm = 7.78 (s, 2H, Ar-O*H*), 7.53 – 7.37 (m, 16H, C*H*^{Ph}), 7.36 – 7.25 (m, 8H, *p*-C*H*^{Ph}) 7.20 – 7.05 (m, 16H, C*H*^{Ph}), 6.87 (t, $^3J_{HH}$ = 7.8 Hz, 2H, Ar-*H*), 6.64 (d, $^3J_{HH}$ = 8.0 Hz, 2H, Ar-*H*), 6.33 (td, $^3J_{HH}$ = 7.8 Hz, 2H, Ar-*H*), 5.61 (d, $^3J_{HH}$ = 8.0 Hz, 2H, Ar-*H*), 4.29 (s, 8H, R$_2$N-C*H*$_2$-PPh$_2$). ^{13}C{^{1}H} NMR (162 MHz, CDCl$_3$): δ_C /ppm = 152.0, 139.7, 133.0, 131.3, 128.8, 128.5, 125.8, 120.2, 116.1, 62.5. ^{31}P{^{1}H} (162 MHz, CDCl$_3$): δ_P /ppm = – 34.3 (s, 2P, RPh$_2$*P*-Re). HR-ESMS: *m/z* calc. for [M]$^+$ at 1229.2905, found at 1229.2935. Selected FT-IR (solid, cm^{-1}): ν (O-H) = 3171 (br), ν_{as} (O=Re=O) = 786 (s) (c.f. [ReO$_2$(dppe)$_2$]I ν_{as} (O=Re=O) = 786 (s).[8])

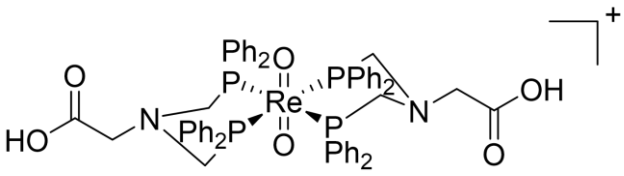

I^- *[ReO₂(κ²-NP₂^PhCOOH^Me)₂]I* (**ReO₂-NP₂COOH**) (**Re-2**): 94 %. ^{1}H NMR (400 MHz, d^3-MeOD): δ_H /ppm = 7.42 (s, 16H, *m*-C*H*^{Ph}), 7.29 (t, $^3J_{HH}$ = 7.5 Hz, 8H, *p*-C*H*^{Ph}), 7.12 (t, $^3J_{HH}$ = 7.5 Hz, 16H, *o*-C*H*^{Ph}), 4.15 (s, 8H, R$_2$N-C*H*$_2$-PPh$_2$), 3.15 (s, 4H, R$_2$N-C*H*$_2$-COOH). ^{13}C{^{1}H} NMR (162 MHz, d^3-MeOD): δ_C /ppm = 174.0, 134.4, 131.9, 130.0, 129.6, 61.8, 49.8. ^{31}P{^{1}H} (162 MHz, d^3-MeOD): δ_P /ppm = – 37.4 (s, 4P, RPh$_2$P-Re). HR-ESMS: *m/z* calc. for [M]$^+$ at 1161.2490, found at 1161.2517. Selected FT-IR (solid, cm^{-1}): ν (O-H) = 3396 (br), ν (C=O) = 1722 (s), ν_{as} (O=Re=O) = 783 (s).

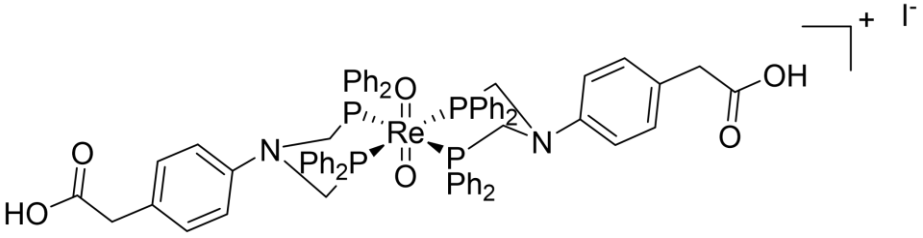

[ReO₂(κ²-NP₂^PhCOOH^Bn)₂]I (**ReO₂-NP₂BnCOOH**) (**Re-3**): 81 %. ^{1}H NMR (400 MHz, d^3-MeOD): δ_H /ppm = 7.34 (t, $^3J_{HH}$ = 7.6 Hz, 24H, *m*-C*H*^{Ph} + *p*-C*H*^{Ph}), 7.16 (t, $^3J_{HH}$ = 7.6 Hz, 16H, *o*-C*H*^{Ph}), 6.88 (d, $^3J_{HH}$ = 8.2 Hz, 4H, *m*-C*H*^{Bn}), 6.36 (d, $^3J_{HH}$ = 8.2 Hz, 4H, *o*-C*H*^{Bn}), 4.53 (s, 8H, R$_2$N-C*H*$_2$-PPh$_2$), 3.36 (s, 4H, Ph-C*H*$_2$-COOH). ^{13}C{^{1}H} NMR (162 MHz, d^3-MeOD): δ_C /ppm = 175.6, 134.8, 132.6, 131.1, 130.0, 129.7, 119.8, 60.5, 40.9. ^{31}P{^{1}H} (162 MHz, d^3-MeOD): δ_P /ppm = – 32.1 (s, 4P, RPh$_2$P-Re). HR-ESMS: *m/z* calc. for [M]$^+$ at 1313.3110, found at 1313.3107. Selected FT-IR (solid, cm^{-1}): ν (O-H) = 3384 (br), ν (C=O) = 1719 (s), ν_{as} (O=Re=O) = 785 (s).

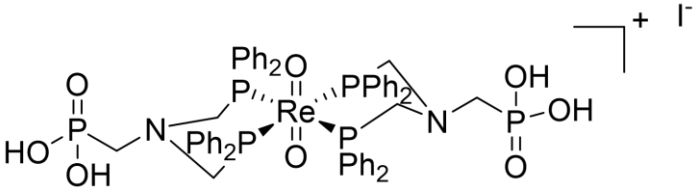

[ReO₂(κ²-NP₂^Ph PO₃H₂^Me)₂]I (**ReO₂-NP₂PO₃H₂**) (**Re-4**):): 64 %. ^{1}H NMR (400 MHz, d^{3}-MeOD): δ_H /ppm = 7.48 (s, 16H, *m*-C*H*^{Ph}), 7.35 (t, $^{3}J_{HH}$ = 7.6 Hz, 8H, *p*-C*H*^{Ph}), 7.17 (t, $^{3}J_{HH}$ = 7.6 Hz, 16H, *o*-C*H*^{Ph}), 4.22 (s, 8H, R$_2$N-C*H*$_2$-PPh$_2$), 3.51 (d, $^{2}J_{HP}$ = 7.0 Hz, 4H, R-*P*O$_3$H$_2$), 2.69 (d, $^{2}J_{HP}$ = 7.2 Hz, 4H, R$_2$N-C*H*$_2$-PO$_3$H$_2$). ^{13}C{^{1}H} NMR (162 MHz, d^{6}-DMSO): δ_C /ppm = 130.7, 128.8, 128.6, 128.3, 60.0, 56.9, 49.5. ^{31}P{^{1}H} (162 MHz, d^{3}-MeOD): δ_P /ppm = + 20.9 (s, 2P, R-*P*O$_3$H$_2$), – 38.7 (s, 4P, RPh$_2$P-Re). HR-ESMS: *m/z* calc. for [M]$^+$ at 1233.2014, found at 1233.2039.Selected FT-IR (solid, cm^{-1}): ν (O-H) = 2891 (br), ν (P=O) = 1285 (s), ν_{as} (O=Re=O) = 782 (s).

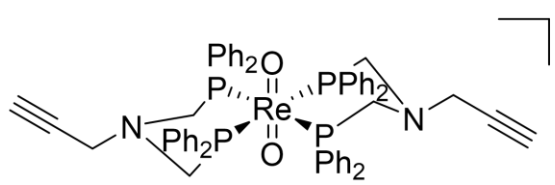

[ReO₂(κ²-NP₂^Ph Prg)₂]I (**ReO₂-NP₂Prg**) (**Re-5**): ^{1}H NMR (400 MHz, CDCl$_3$): 72 %. δ_H /ppm = 7.49 – 7.31 (m, 24H, *m*-C*H*^{Ph} + *p*-C*H*^{Ph}), 7.14 (t, $^{3}J_{HH}$ = 7.6 Hz, 16H, *o*-C*H*^{Ph}), 3.79 (s, 8H, R$_2$N-C*H*$_2$-PPh$_2$), 3.19 (d, $^{4}J_{HH}$ = 2.4 Hz, 4H, R$_2$N-C*H*$_2$-R), 2.28 (t, $^{4}J_{HH}$ = 2.4 Hz, 2H, R-C*H*). ^{13}C{^{1}H} NMR (162 MHz, CDCl$_3$): δ_C /ppm = 132.8, 131.3, 129.1, 128.8, 76.5, 75.5, 60.2, 51.6. ^{31}P{^{1}H} (162 MHz, CDCl$_3$): δ_P /ppm = – 34.5 (s, 4P, RPh$_2$P-Re). HR-ESMS: *m/z* calc. for [M]$^+$ at 1121.2693, found at 1121.2704. Selected FT-IR (solid, cm^{-1}): ν (CC) = 2100 (w), 2082 (w), ν_{as} (O=Re=O) = 784 (s).

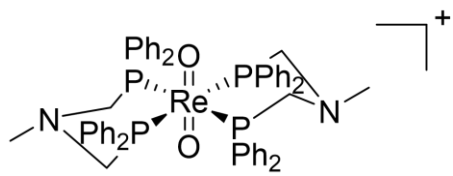

[ReO₂(κ²-NP₂^Ph Me)₂]I (**ReO₂-NP₂Me**) (**Re-6**): ^{1}H NMR (400 MHz, d^{3}-MeOD): 88 %. δ_H /ppm = 7.42 (s, 18H, *m*-C*H*^{Ph}), 7.34 (t, $^{3}J_{HH}$ = 7.6 Hz, 8H, *p*-C*H*^{Ph}), 7.15 (t, $^{3}J_{HH}$ = 7.6 Hz, 16H, o-C*H*^{Ph}), 3.84 (s, 8H, R$_2$N-C*H*$_2$-PPh$_2$), 2.26 (s, 6H, R$_2$N-C*H*$_3$). ^{13}C NMR (162 MHz, CDCl$_3$): δ_C /ppm = 132.8, 131.1, 129.3, 128.7, 62.2., 50.3. ^{31}P{^{1}H} (162 MHz, d^{3}-MeOD): δ_P /ppm = – 37.4 (s, 4P, RPh$_2$P-Re). HR-ESMS: *m/z* calc. for [M]$^+$ at 1073.2693, found at 1073.2690. Selected FT-IR (solid, cm^{-1}): ν_{as} (O=Re=O) = 783 (s).

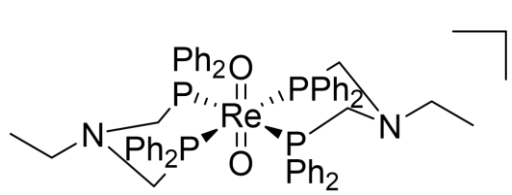

[ReO₂(κ²-NP₂^Ph Et)₂]I (**ReO₂-NP₂Et**) (**Re-7**): ^{1}H NMR (400 MHz, d^{3}-MeOD): 57 %. δ_H /ppm = 7.47 – 7.36 (m, 16H, *m*-C*H*^{Ph}), 7.36 – 7.29 (m, 8H, *p*-C*H*^{Ph}) 7.18 – 7.09 (m, 16H, *o*-C*H*^{Ph}), 3.85 (s, 8H, R$_2$N-C*H*$_2$-PPh$_2$), 2.50 (q, $^{3}J_{HH}$ = 7.0 Hz, 4H, R$_2$N-C*H*$_2$-CH$_3$), 0.68 (t, $^{3}J_{HH}$ = 7.0 Hz, 6H, R$_2$N-CH$_2$-C*H*$_3$). ^{13}C{^{1}H} NMR (162 MHz, CDCl$_3$): δ_C /ppm = 133.0, 131.1, 128.7, 128.6, 60.8, 56.4, 10.4. ^{31}P{^{1}H} (162 MHz, d^{3}-MeOD): δ_P /ppm = – 36.2 (s, 4P, RPh$_2$P-Re). HR-ESMS: *m/z*

calc. for $[M]^+$ at 1103.3006, found at 1103.3033. Selected FT-IR (solid, cm^{-1}): ν_{as} (O=Re=O) = 784 (s).

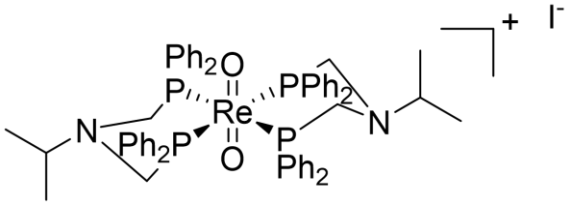

[ReO$_2$(κ^2-NP$_2^{Ph}$iPr)$_2$]I (**ReO$_2$-NP$_2$iPr**) (**Re-8**): ^{1}H NMR (400 MHz, $CDCl_3$): 69 %. δ_H /ppm = 7.48 – 7.18 (m, 24H, *m*-C*H*^{Ph} + *o*-C*H*^{Ph}), 7.18 – 6.97 (m, 16H, *p*-C*H*^{Ph}), 3.66 (s, 8H, Ph_2P-CH_2-N), 2.61 (hp, 2H, N-C*H*-$(CH_3)_2$, $^3J_{HH}$ = 6.6 Hz), 0.62 (d, 12H, N-CH-(CH_3)$_2$, $^3J_{HH}$ = 6.6 Hz). $^{13}C\{^1H\}$ NMR (162 MHz, $CDCl_3$): δ_C /ppm = 133.3, 131.2, 129.4, 128.5, 60.2, 59.1, 17.7. $^{31}P\{^1H\}$ (162 MHz, $CDCl_3$): δ_P /ppm = – 36.1 (s, 4P, Re-*P*Ph_2R). HR-MS: m/z calc. for $[M]^+$ at 1129.3319, found at 1129.3347. Selected FT-IR (solid, cm^{-1}): ν_{as} (O=Re=O) = 781 (s).

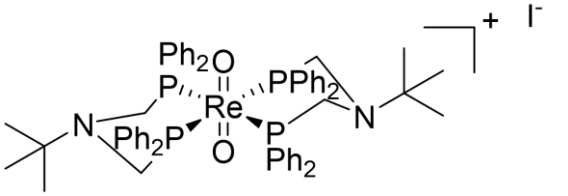

[ReO$_2$(κ^2-NP$_2^{Ph}$tBu)$_2$]I (**ReO$_2$-NP$_2$tBu**) (**Re-9**): 32 %. ^{1}H NMR (400 MHz, $CDCl_3$) δ_H /ppm = 7.42 – 7.28 (m, 24H, *m*-C*H*^{Ph} + *o*-C*H*^{Ph}), 7.17 – 7.07 (m, 16H, *p*-C*H*^{Ph}), 3.67 (s, 8H, Ph_2P-CH_2-N), 0.70 (s, 18H, N-C-$(CH_3)_3$). $^{13}C\{^1H\}$ NMR (162 MHz, $CDCl_3$): δ_C /ppm = 133.9, 131.3, 129.0, 128.4, 58.6, 57.4, 26.2. $^{31}P\{^1H\}$ (162 MHz, $CDCl_3$): δ_P /ppm = – 36.1 (s, 4P, Re-*P*Ph_2R). HR-MS: m/z calc. for $[M]^+$ at 1157.3632, found at 1157.3663. Selected FT-IR (solid, cm^{-1}): ν_{as} (O=Re=O) = 782 (s).

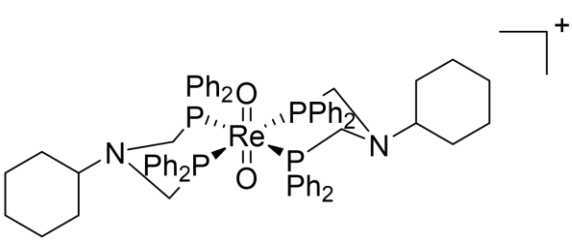

[ReO$_2$(κ^2-NP$_2^{Ph}$Cyh)$_2$]I (**ReO$_2$-NP$_2$Cyh**) (**Re-10**): 78 %. ^{1}H NMR (400 MHz, $CDCl_3$) δ_H /ppm = 7.42 – 7.22 (m, 24H, *m*-C*H*^{Ph} + *o*-C*H*^{Ph}), 7.17 – 7.03 (m, 16H, *p*-C*H*^{Ph}), 3.73 (s, 8H, Ph_2P-CH_2-N), 2.19 – 2.07 (m, 2H, N-C*H*-R_2), 1.90 – 0.74 (m, 20H, N-CH-((CH_2-CH_2)$_2$-CH_2)). $^{13}C\{^1H\}$ NMR (162 MHz, $CDCl_3$): δ_C /ppm = 133.2, 131.0, 129.2, 128.4, 69.4, 59.7, 28.4, 25.8, 25.6. $^1P\{^1H\}$ (162 MHz, $CDCl_3$): δ_P /ppm = – 36.2 (s, 4P, Re-*P*Ph_2R). HR-MS: m/z calc. for $[M]^+$ at 1209.3940, found at 1209.3958. Selected FT-IR (solid, cm^{-1}): ν_{as} (O=Re=O) = 784 (s).

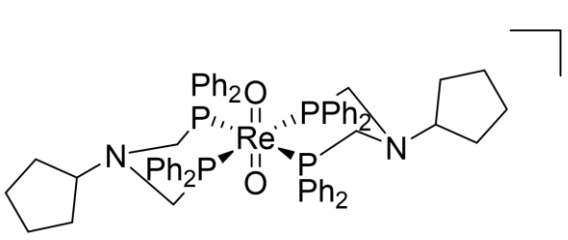

[ReO$_2$(κ^2-NP$_2^{Ph}$Cyp)$_2$]I (**ReO$_2$-NP$_2$Cyp**) (**Re-11**): 68 %. ^{1}H NMR (400 MHz, $CDCl_3$) δ_H /ppm = 7.37 – 7.27 (m, 24H, *m*-C*H*^{Ph} + *o*-C*H*^{Ph}), 7.17 – 7.06 (m, 16H, *p*-C*H*^{Ph}), 3.71 (s, 8H, Ph_2P-CH_2-N), 2.86 – 2.73 (m, 2H, N-C*H*-R_2), 1.45 – 1.19 (m, 16H, N-CH-(CH_2-CH_2)$_2$). $^{13}C\{^1H\}$ NMR (162 MHz, $CDCl_3$): δ_C /ppm = 133.3, 131.2, 129.2, 128.5, 71.5, 60.0, 27.4, 23.0. $^{31}P\{^1H\}$ (162 MHz, $CDCl_3$): δ_P /ppm

= – 36.2 (s, 4P, Re-*P*Ph$_2$R). HR-MS: m/z calc. for [M]$^+$ at 1181.3627, found at 1181.3661. Selected FT-IR (solid, cm^{-1}): ν_{as} (O=Re=O) = 785 (s).

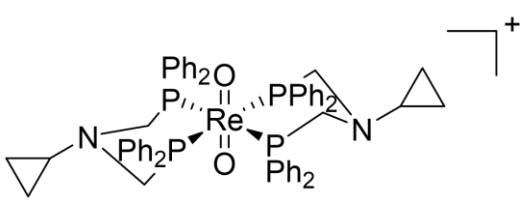

[ReO$_2$(κ^2-NP$_2^{Ph}$Cypr)$_2$]I (**ReO$_2$-NP$_2$Cypr**) (**Re-12**): 89 %. ^{1}H NMR (400 MHz, CDCl$_3$) δ_H /ppm = 7.49 – 7.35 (m, 16H, *m*-C*H*^{Ph}), 7.35 – 7.28 (m, 8H, *o*-C*H*^{Ph}), 7.16 – 7.07 (m, 16H, *p*-C*H*^{Ph}), 3.95 (s, 8H, Ph$_2$P-C*H*$_2$-N), 1.65 – 1.60 (m, 2H, N-C*H*-R$_2$), 0.22 – 0.14 (m, 4H, N-CH-(C*(H)*(H)-C*(H)*(H))$_2$), -0.01 – -0.08 (m, 4H, N-CH-(C(H)(*H*)-C(H)(*H*))$_2$). ^{13}C{^{1}H} NMR (162 MHz, CDCl$_3$): δ_C /ppm = 133.4, 131.2, 129.1, 128.6, 61.1, 46.9, 8.7. ^{31}P{^{1}H} (162 MHz, CDCl$_3$): δ_P /ppm = – 42.6 (s, 4P, Re-*P*Ph$_2$R). HR-MS: m/z calc. for [M]$^+$ at 1125.3001, found at 1125.3029. Selected FT-IR (solid, cm^{-1}): ν_{as} (O=Re=O) = 784 (s).

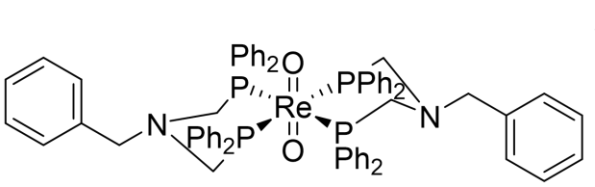

[ReO$_2$(κ^2-NP$_2^{Ph}$Bn)$_2$]I (**ReO$_2$-NP$_2$Bn**) (**Re-13)**:): 48 %. ^{1}H NMR (400 MHz, CDCl$_3$) δ_H /ppm = 7.36 – 7.20 (m, 24H, *m*-C*H*^{Ph} + *o*-C*H*^{Ph}), 7.17 (t, 2H, *p*-C*H*^{Bn}, ^{3}J$_{HH}$ = 7.4 Hz), 7.12 – 6.98 (m, 20H, *p*-C*H*^{Ph} + *m*-C*H*^{Bn}), 6.57 (d, 4H, *o*-C*H*^{Bn}, ^{3}J$_{HH}$ = 7.6 Hz), 3.78 (s, 8H, Ph$_2$P-C*H*$_2$-N), 3.47 (s, 4H, N-C*H*$_2$-Ph). ^{13}C{^{1}H} NMR (162 MHz, CDCl$_3$): δ_C /ppm = 135.7, 133.0, 131.0, 129.5, 128.6, 127.9, 66.8, 60.9. ^{31}P{^{1}H} (162 MHz, CDCl$_3$): δ_P /ppm = – 36.5 (s, 4P, Re-*P*Ph$_2$R). HR-MS: m/z calc. for [M]$^+$ at 1225.3314, found at 1225.3334. Selected FT-IR (solid, cm^{-1}): ν_{as} (O=Re=O) = 785 (s).

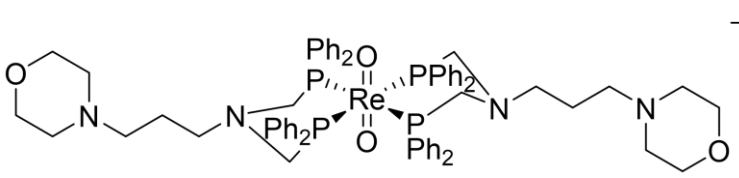

[ReO$_2$(κ^2-NP$_2^{Ph}$Mor^{Pr})$_2$]I (**ReO$_2$-NP$_2$Mor**) (**Re-14**): 72 %. ^{1}H NMR (400 MHz, CDCl$_3$) δ_H /ppm = 7.43 – 7.23 (m, 24H, *m*-C*H*^{Ph} + *o*-C*H*^{Ph}), 7.17 – 7.03 (m, 16H, *p*-C*H*^{Ph}), 3.79 (s, 8H, Ph$_2$P-C*H*$_2$-N), 3.70 – 3.61 (m, 8H, N-(CH$_2$-C*H*$_2$)$_2$-O), 2.46 (t, 4H, ^{3}J$_{HH}$ = 7.5 Hz, N-C*H*$_2$-CH$_2$-CH$_2$-Mor), 2.39 – 2.26 (m, 8H, N-(C*H*$_2$-CH$_2$)$_2$-O), 2.01 (t, 4H, ^{3}J$_{HH}$ = 7.1 Hz, N-CH$_2$-CH$_2$-C*H*$_2$-Mor), 1.39 (tt, 4H, ^{3}J$_{HH}$ = 7.5 Hz, ^{3}J$_{HH}$ = 7.1 Hz, N-CH$_2$-C*H*$_2$-CH$_2$-Mor). ^{13}C{^{1}H} NMR (162 MHz, CDCl$_3$): δ_C /ppm = 133.1, 131.1, 128.6, 66.1, 61.3, 59.9, 55.8, 53.2, 22.4. ^{31}P{^{1}H} (162 MHz, CDCl$_3$): δ_P /ppm = – 36.9 (s, 4P, Re-*P*Ph$_2$R). HR-MS: m/z calc. for [M]$^+$ at 1299.4369, found at 1299.4366. Selected FT-IR (solid, cm^{-1}): ν_{as} (O=Re=O) = 785 (s).

S4) NMR and Mass Spectra for $[ReO_2(NP_2^{Ph}X^R)_2]I$ Complexes

Figure S1: ^1H NMR spectrum (d^3-MeOD, 400 MHz, 298 K) of **ReO_2-NP_2OH** (**Re-1**). Asterisks indicate solvent impurities.

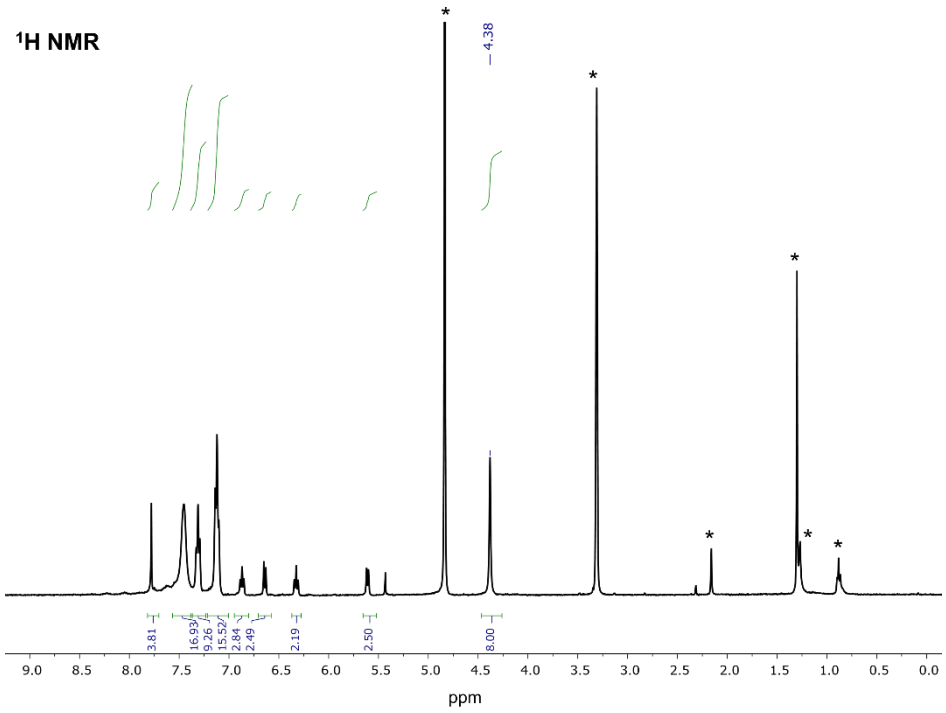

Figure S2: $^{31}P\{^1H\}$ NMR spectrum ($CDCl_3$, 400 MHz, 298 K) of **ReO_2-NP_2OH** (**Re-1**)

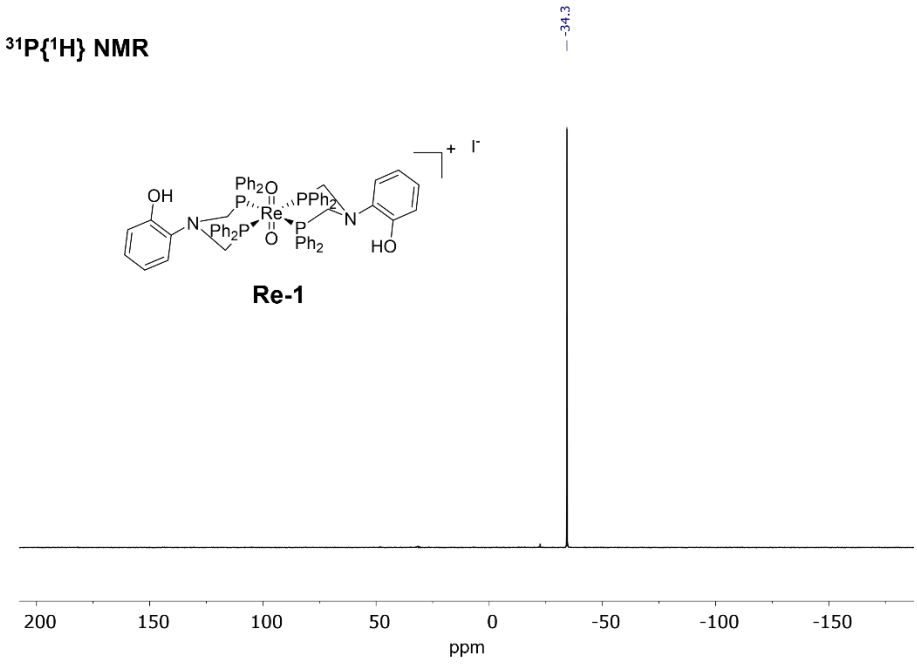

Figure S3: $^{13}C\{^{1}H\}$ NMR spectrum ($CDCl_3$, 400 MHz, 298 K) of **ReO_2-NP_2OH** (**Re-1**). Asterisks indicate solvent impurities.

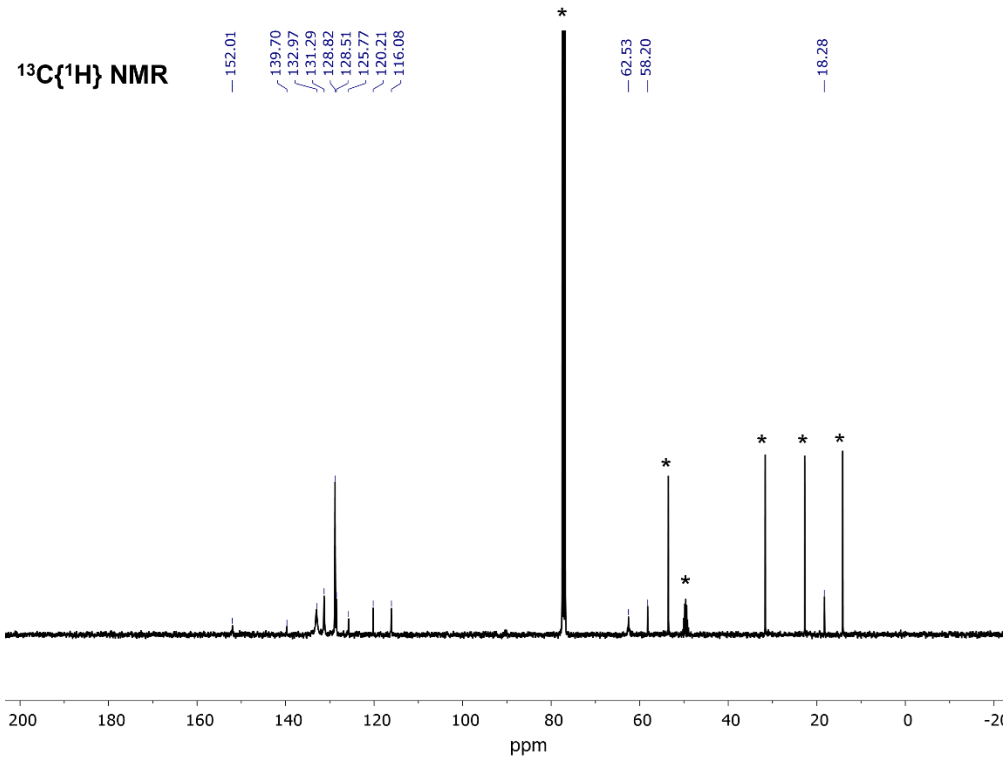

Figure S4: High resolution ES-MS spectrum for **ReO_2-NP_2OH** (**Re-1**)

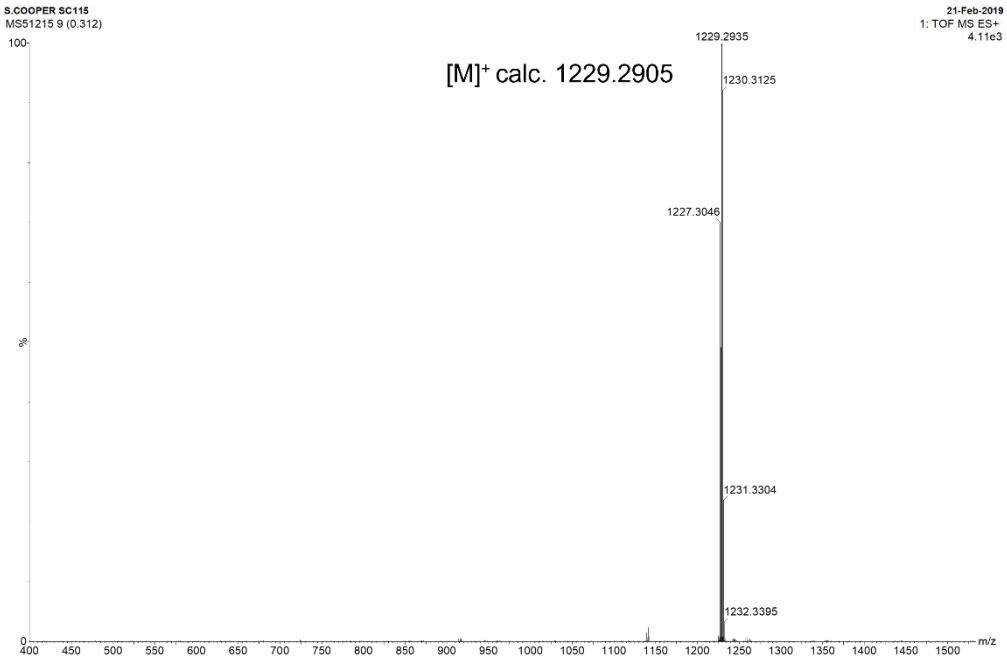

Figure S5: ^{1}H NMR spectrum (d^{3}-MeOD, 400 MHz, 298 K) of **ReO_2-NP_2COOH** (**Re-2**). Asterisks indicate solvent impurities.

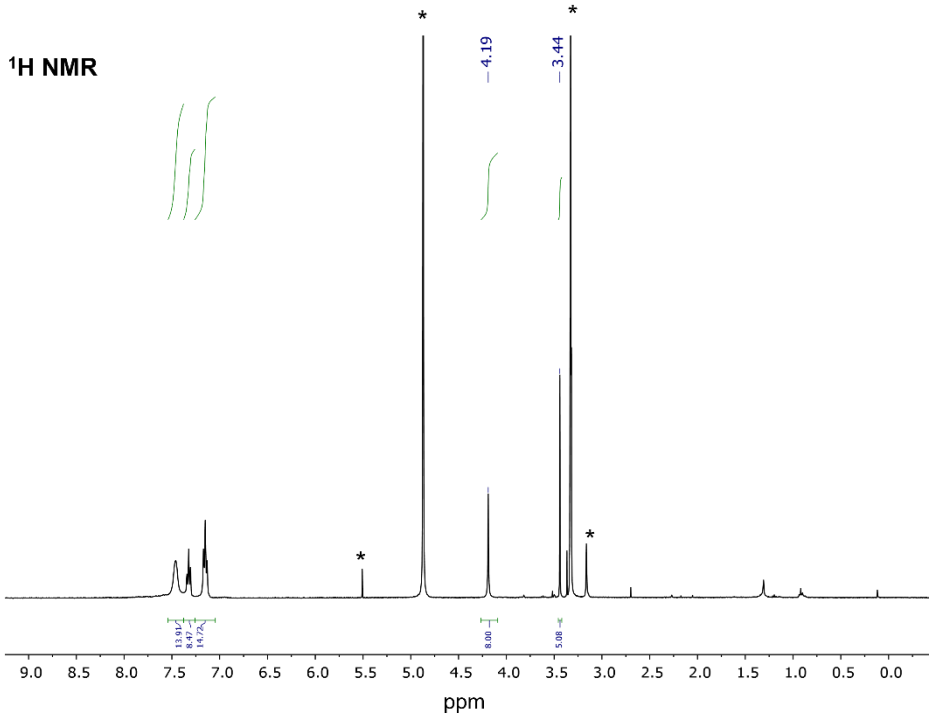

Figure S6: ^{31}P{^{1}H} NMR spectrum (d^{3}-MeOD, 400 MHz, 298 K) of **ReO_2-NP_2COOH** (**Re-2**).

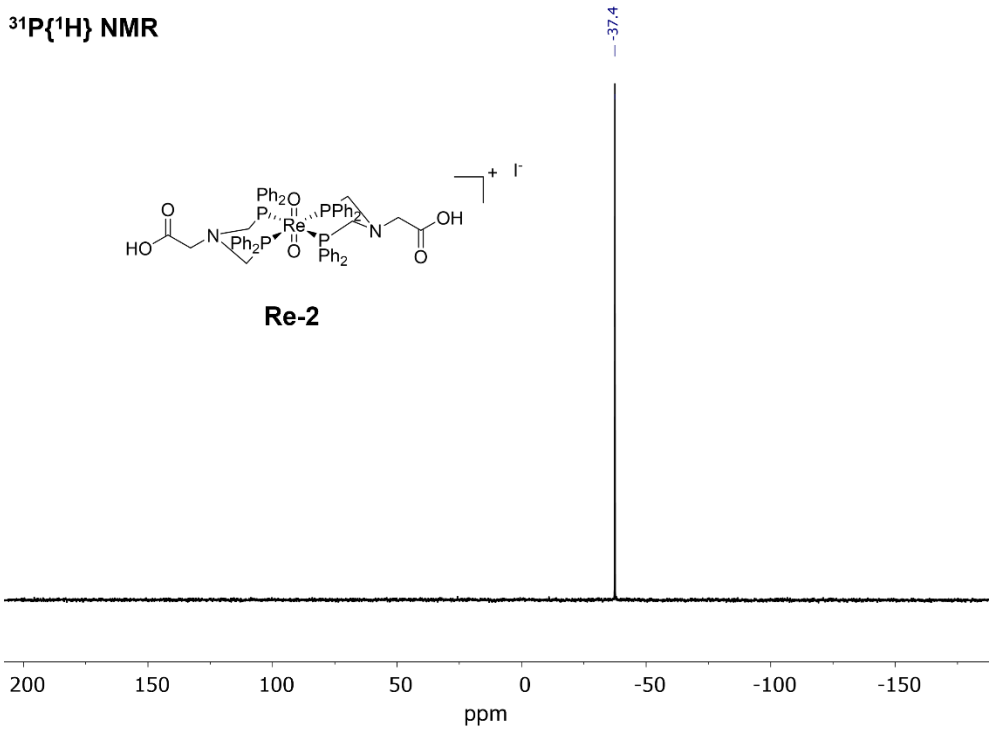

Figure S7: $^{13}C\{^{1}H\}$ NMR spectrum (d^3-MeOD, 400 MHz, 298 K) of **ReO_2-NP_2COOH** (**Re-2**). Asterisks indicate solvent impurities.

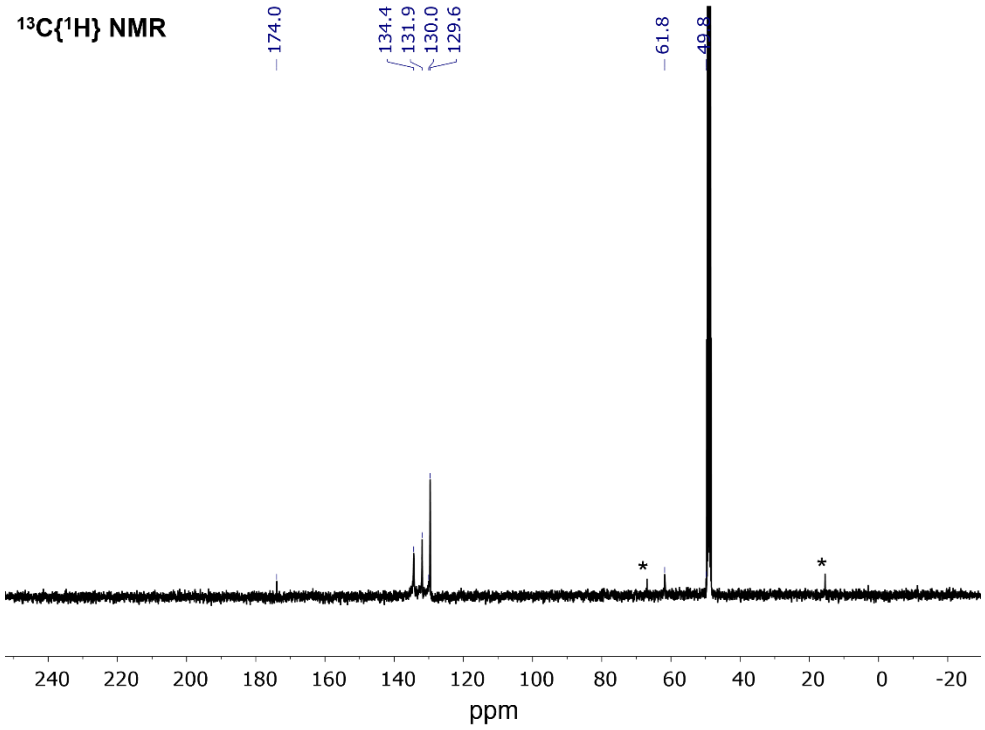

Figure S8: High resolution ES-MS spectrum for **ReO_2-NP_2COOH** (**Re-2**)

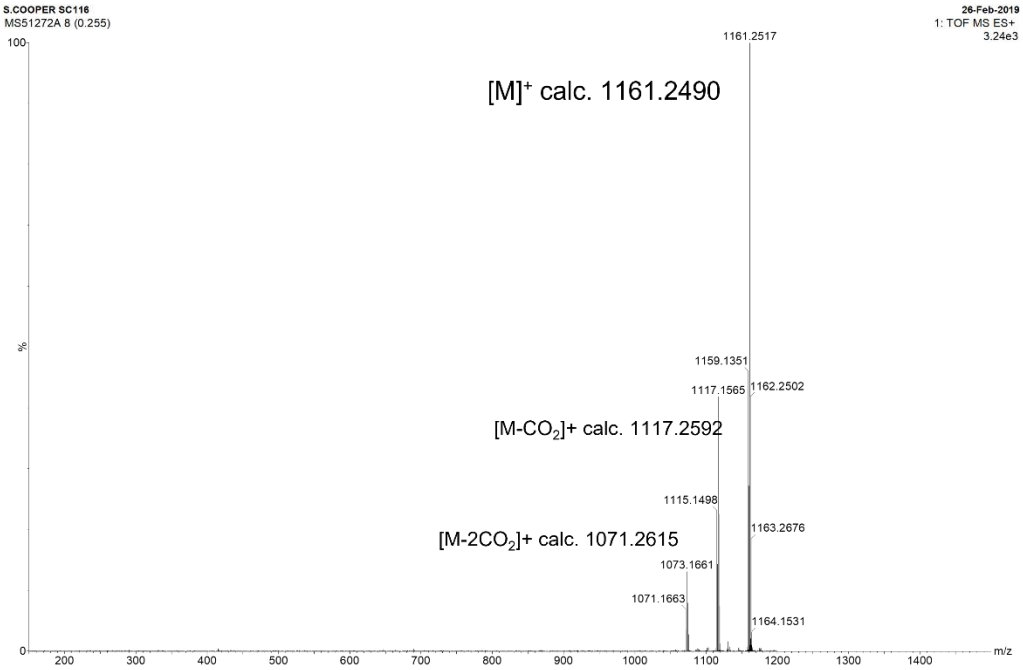

Figure S9: ^{1}H NMR spectrum (d^{3}-MeOD, 400 MHz, 298 K) of **ReO_2-NP_2BnCOOH** (**Re-3**). Asterisks indicate solvent impurities.

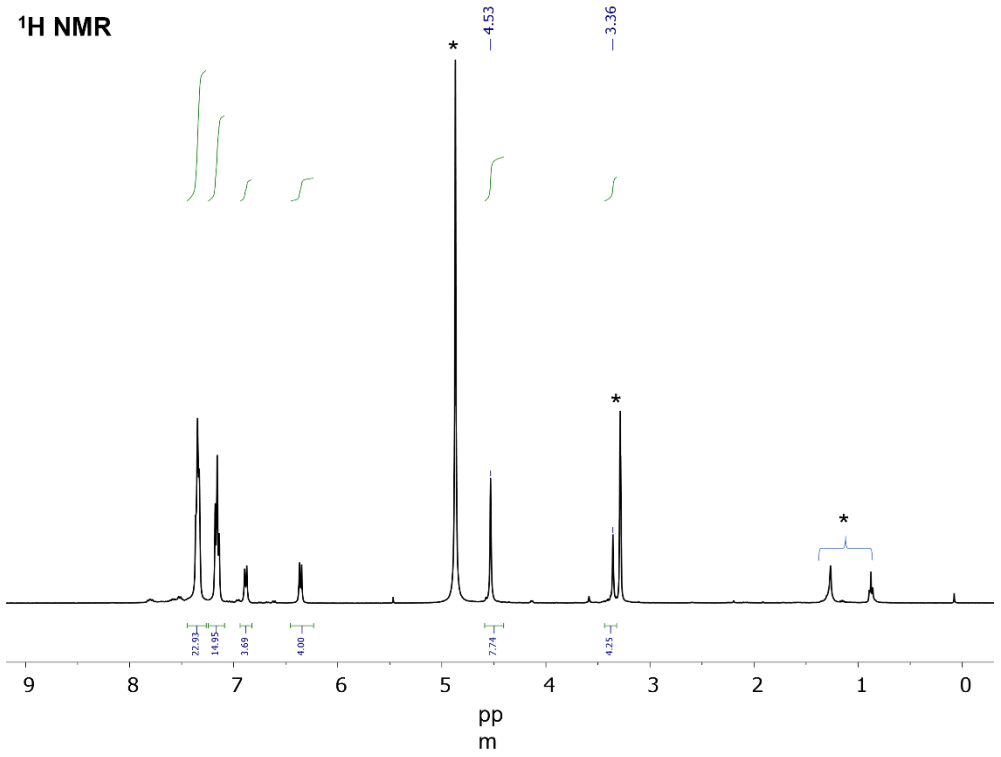

Figure S10: ^{31}P{^{1}H} NMR spectrum (d^{3}-MeOD, 400 MHz, 298 K) of **ReO_2-NP_2BnCOOH** (**Re-3**).

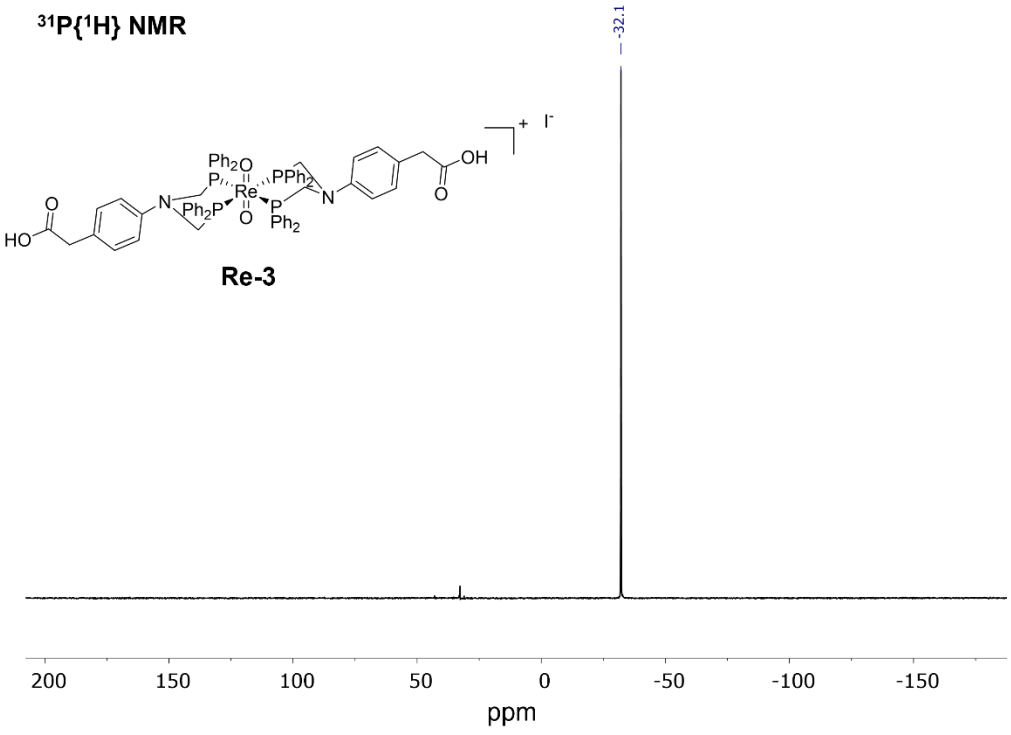

Figure S11: $^{13}C\{^{1}H\}$ NMR spectrum (d^3-MeOD, 400 MHz, 298 K) of **ReO_2-NP_2BnCOOH** (**Re-3**). Asterisks indicate solvent impurities.

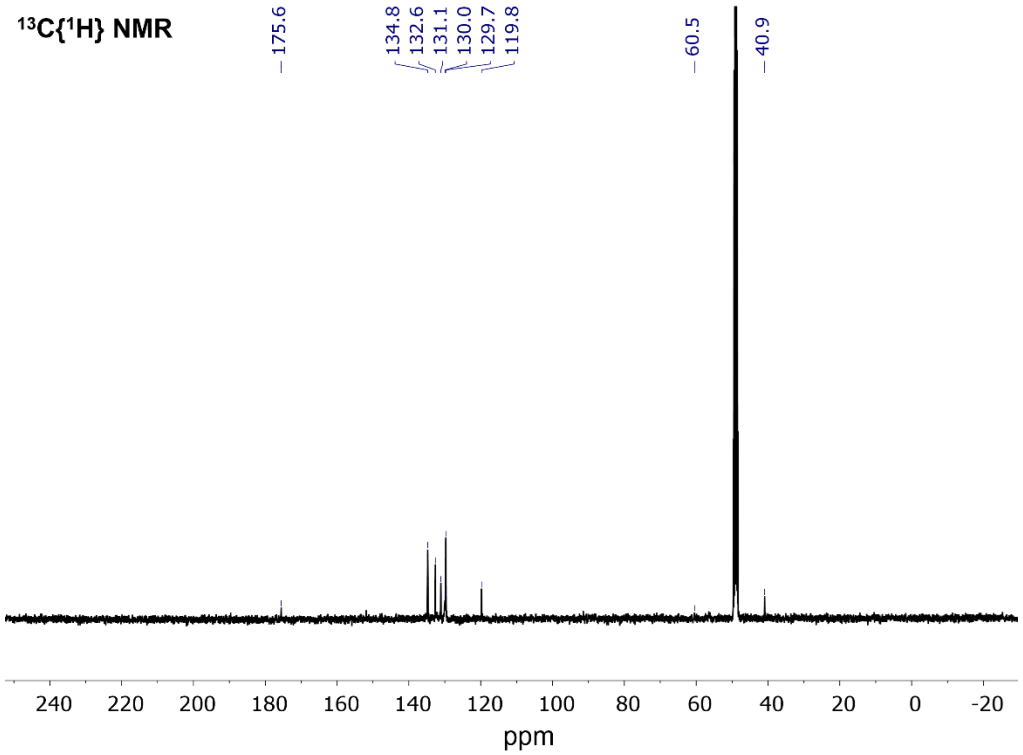

Figure S12: High resolution ES-MS spectrum for **ReO_2-NP_2BnCOOH** (**Re-3**)

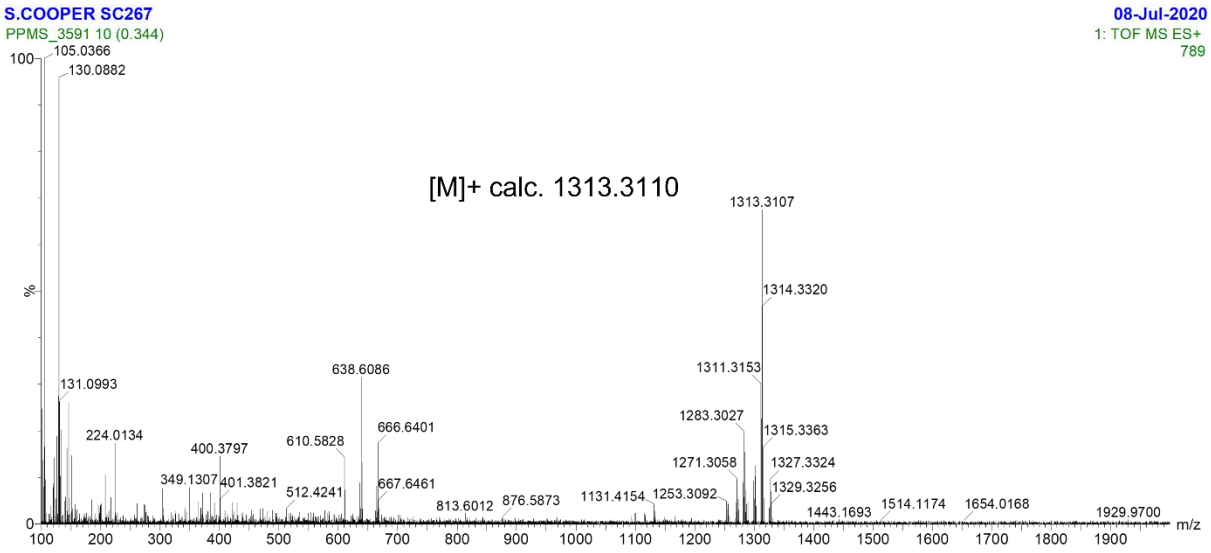

Figure S13: ^{1}H NMR spectrum (d^{3}-MeOD, 400 MHz, 298 K) of **ReO_2-$NP_2PO_3H_2$** (**Re-4**). Asterisks indicate solvent impurities.

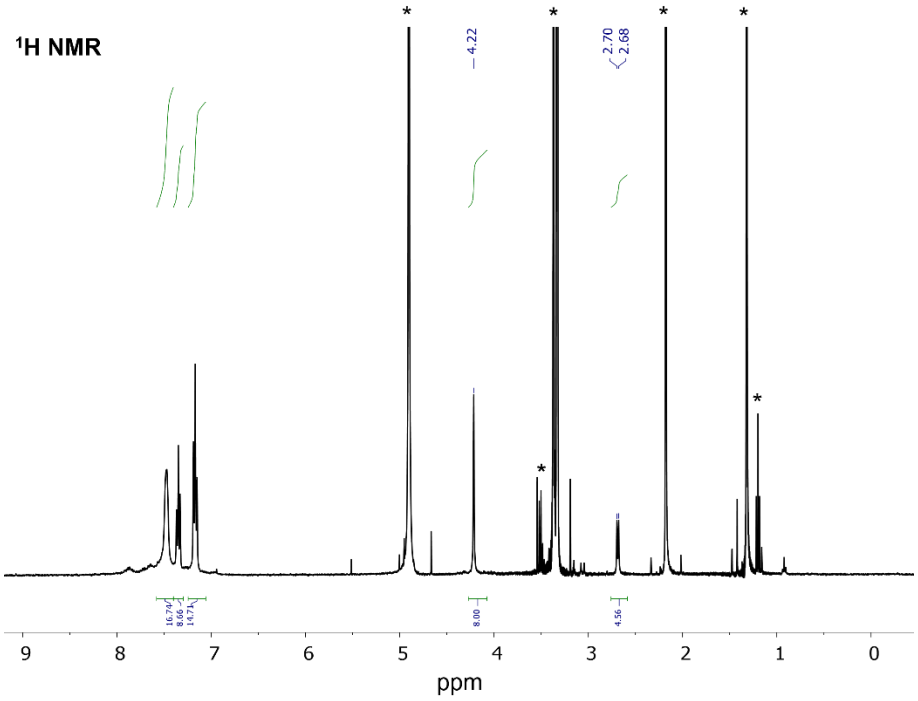

Figure S14: ^{31}P{^{1}H} NMR spectrum (d^{3}-MeOD, 400 MHz, 298 K) of **ReO_2-$NP_2PO_3H_2$** (**Re-4**). Asterisks indicate small (< 1 %) additional impurities.

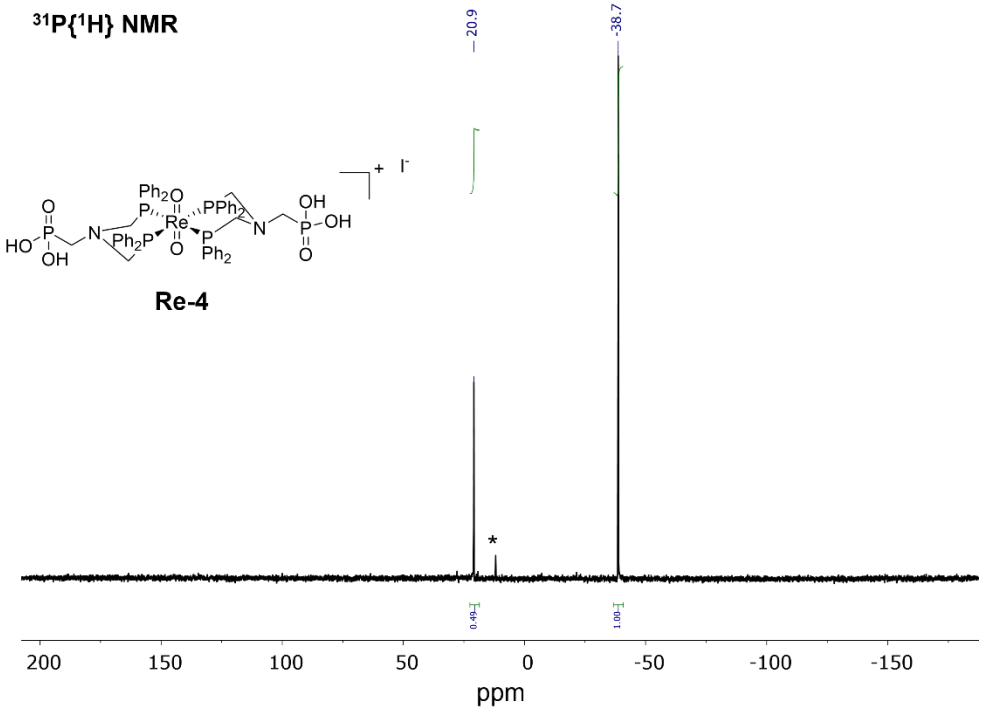

Figure S15: High resolution ES-MS spectrum for **ReO_2-$NP_2PO_3H_2$** (**Re-4**)

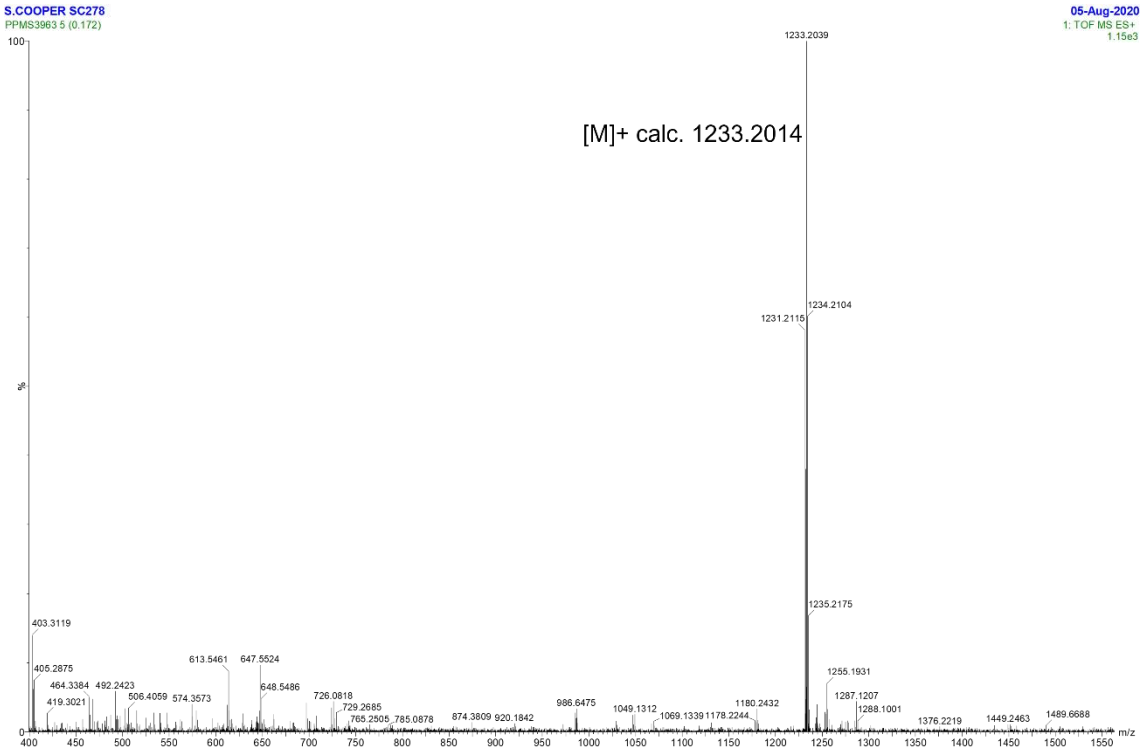

Figure S16: $^{13}C\{^1H\}$ NMR spectrum (d^6-DMSO, 400 MHz, 298 K) of **ReO_2-$NP_2PO_3H_2$** (**Re-4**). Asterisks indicate solvent impurities.

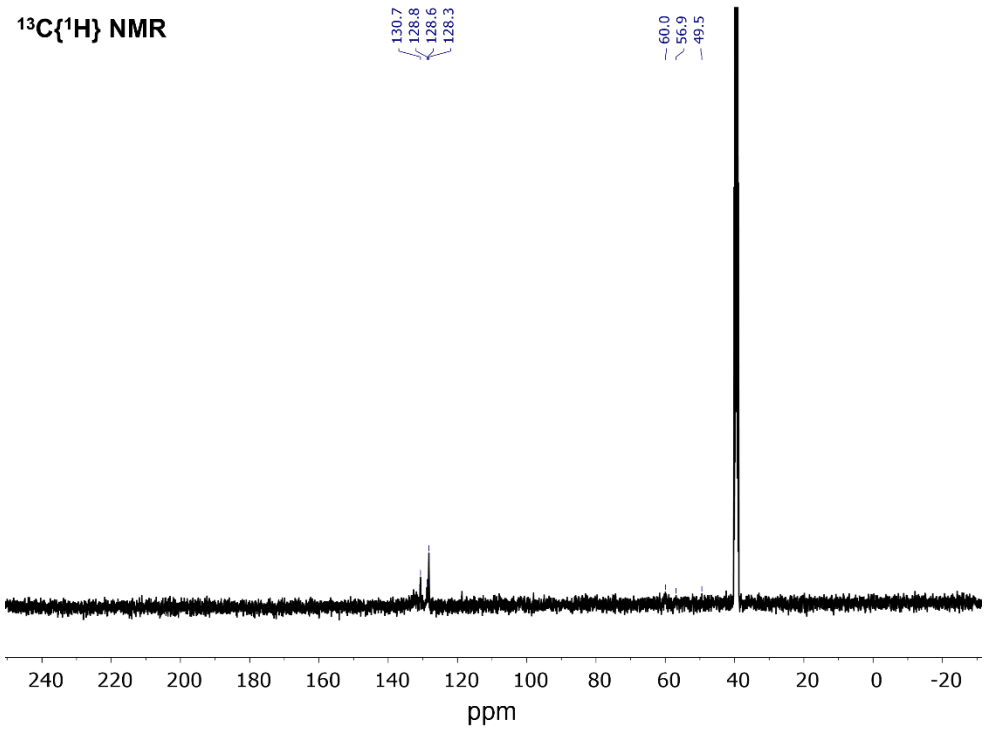

Figure S17: ^{1}H NMR spectrum ($CDCl_3$, 400 MHz, 298 K) of **ReO_2-NP_2Prg** (**Re-5**). Asterisks indicate solvent impurities.

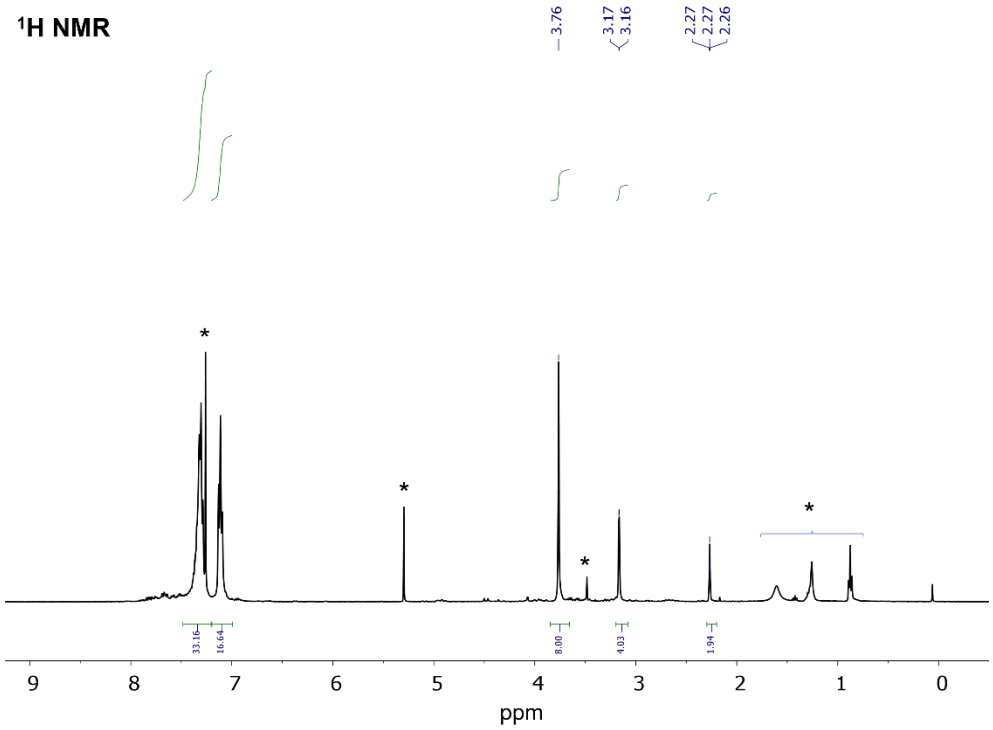

Figure S18: ^{31}P{^{1}H} NMR spectrum ($CDCl_3$, 400 MHz, 298 K) of **ReO_2-$NP_2PO_3H_2$** (**Re-4**).

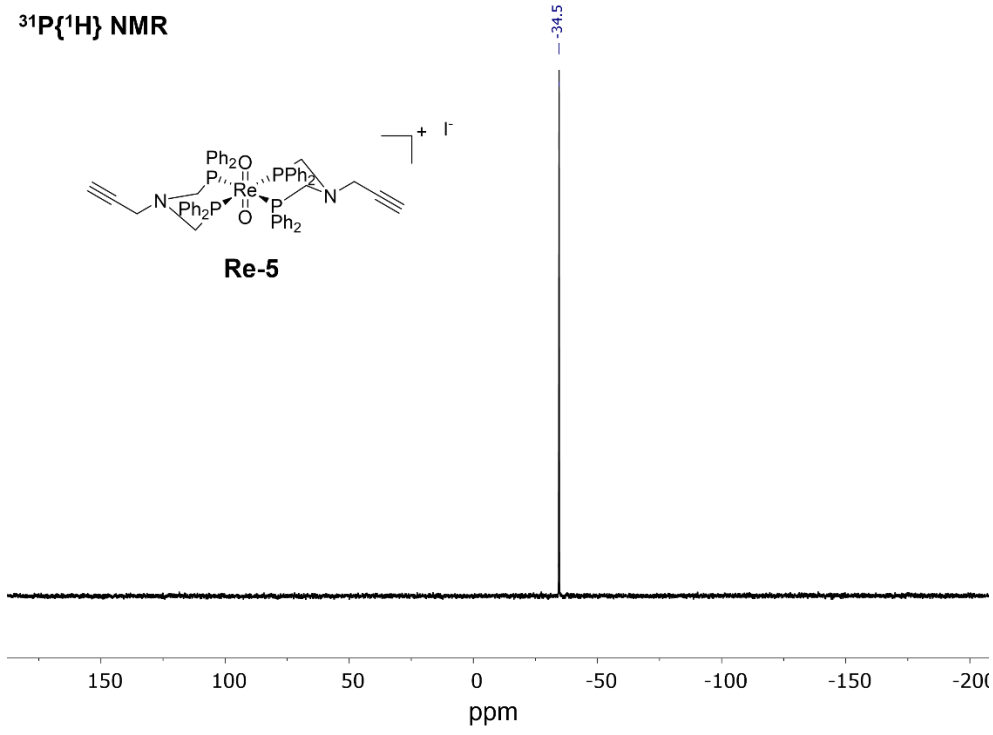

Figure S19: $^{13}C\{^{1}H\}$ NMR spectrum ($CDCl_3$, 400 MHz, 298 K) of **ReO_2-NP_2Prg** (**Re-5**). Asterisks indicate solvent impurities.

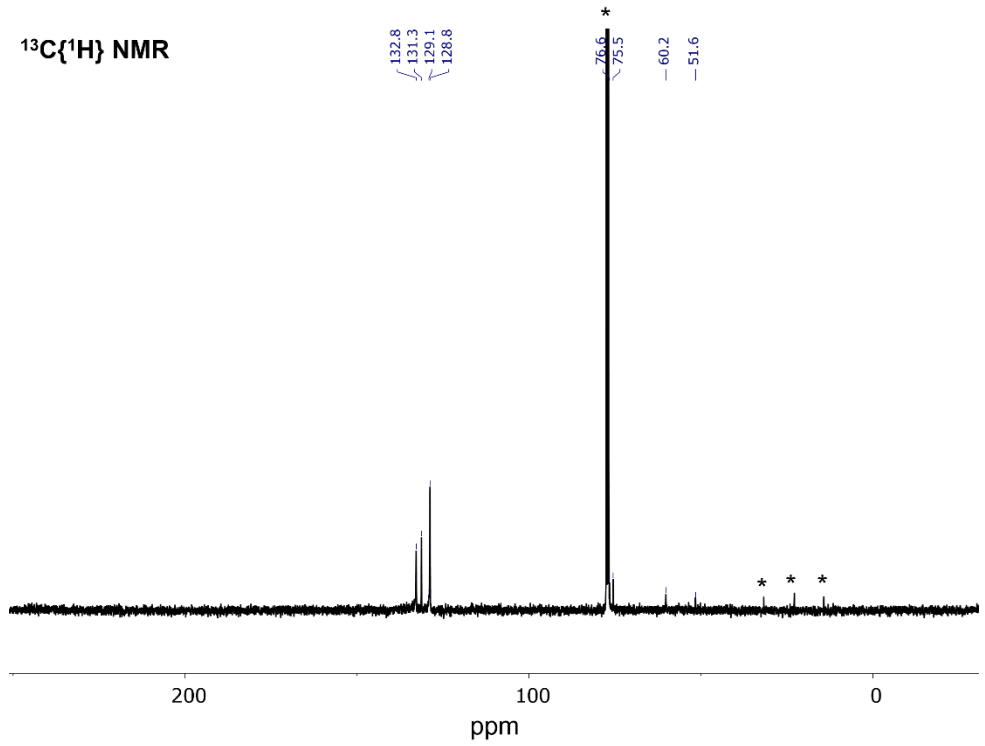

Figure S20: High resolution ES-MS spectrum for **ReO_2-NP_2Prg** (**Re-5**)

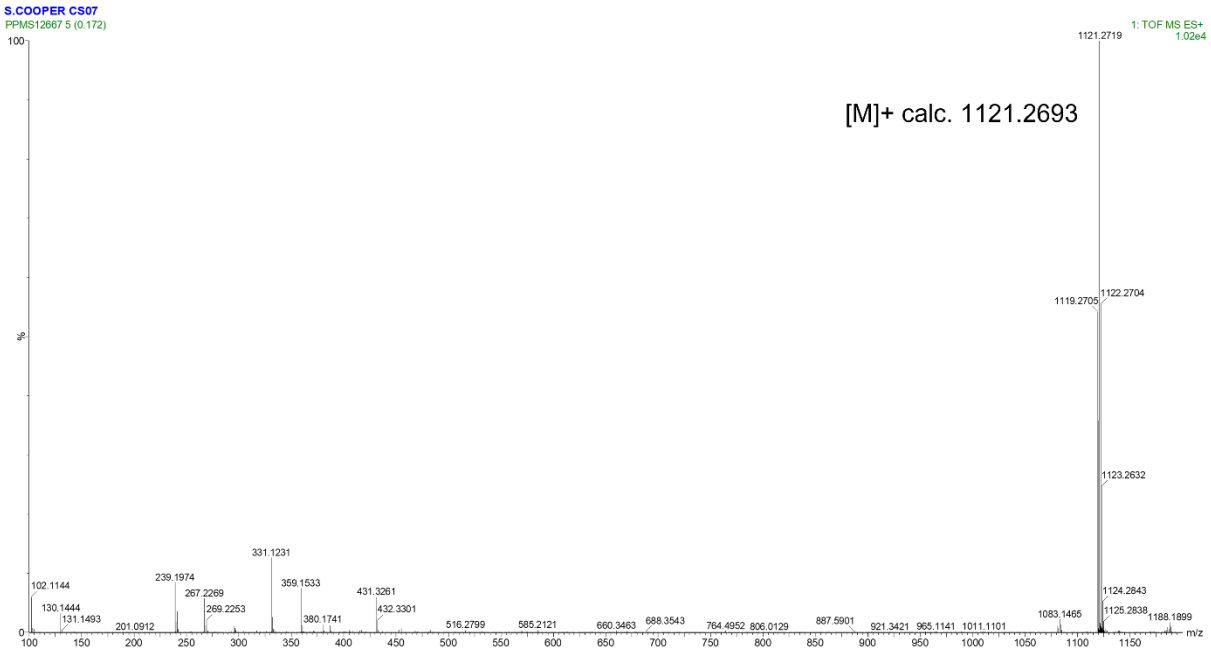

Figure S21: ^{1}H NMR spectrum (d^{3}-MeOD, 400 MHz, 298 K) of **ReO_2-NP_2Me** (**Re-6**). Asterisks indicate solvent impurities.

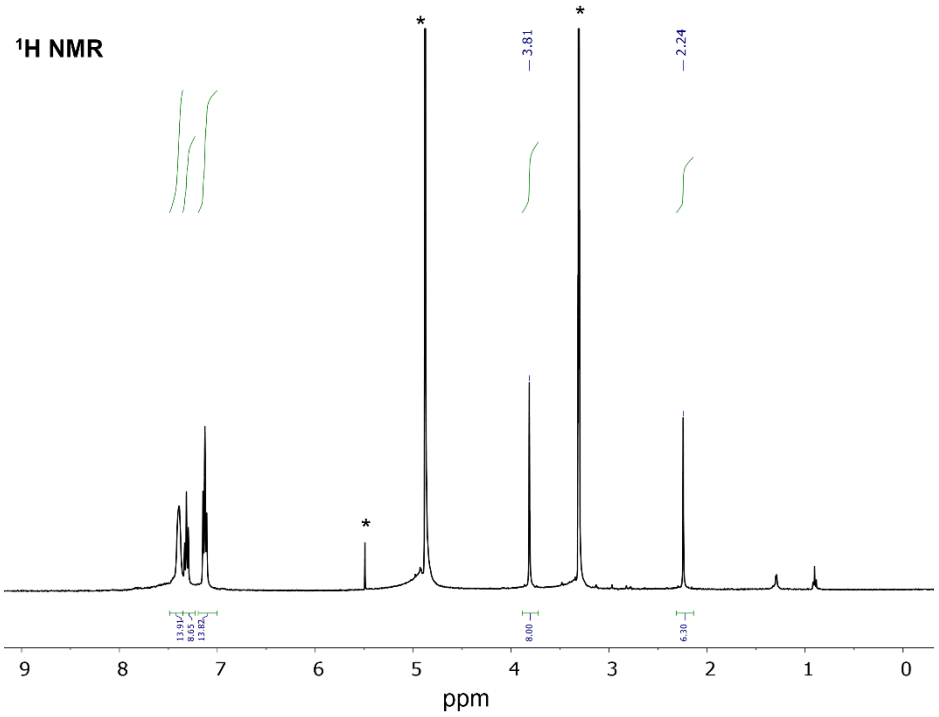

Figure S22: ^{31}P{^{1}H} NMR spectrum (d^{3}-MeOD, 400 MHz, 298 K) of **ReO_2-NP_2Me** (**Re-6**).

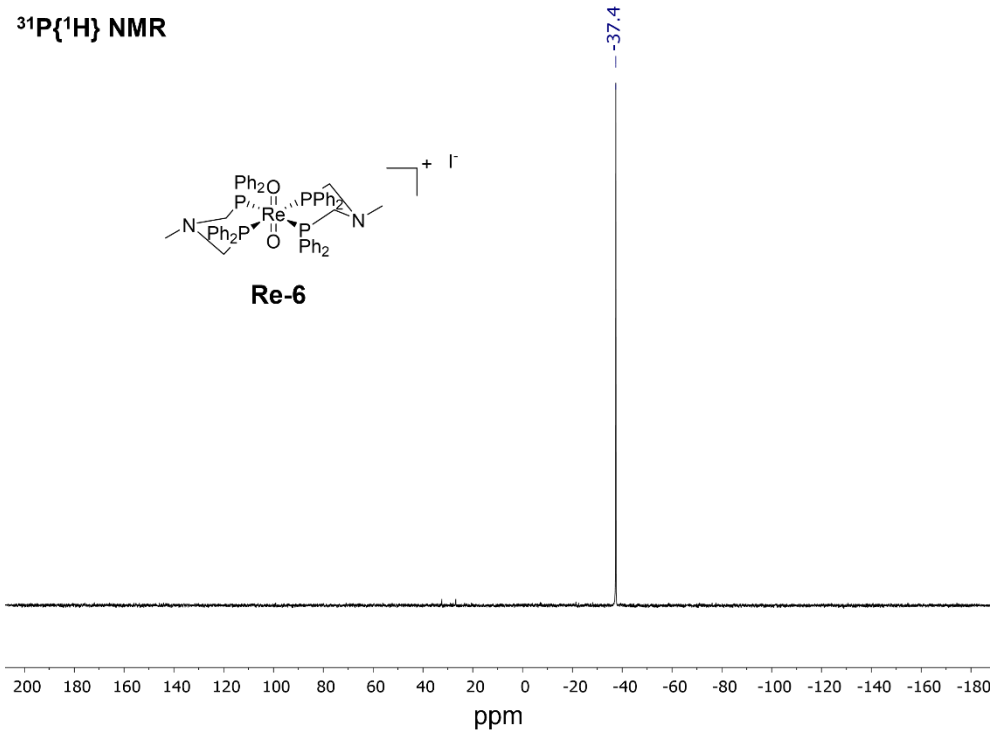

Figure S23: $^{13}C\{^{1}H\}$ NMR spectrum ($CDCl_3$, 400 MHz, 298 K) of **ReO_2-NP_2Me** (**Re-6**). Asterisks indicate solvent impurities.

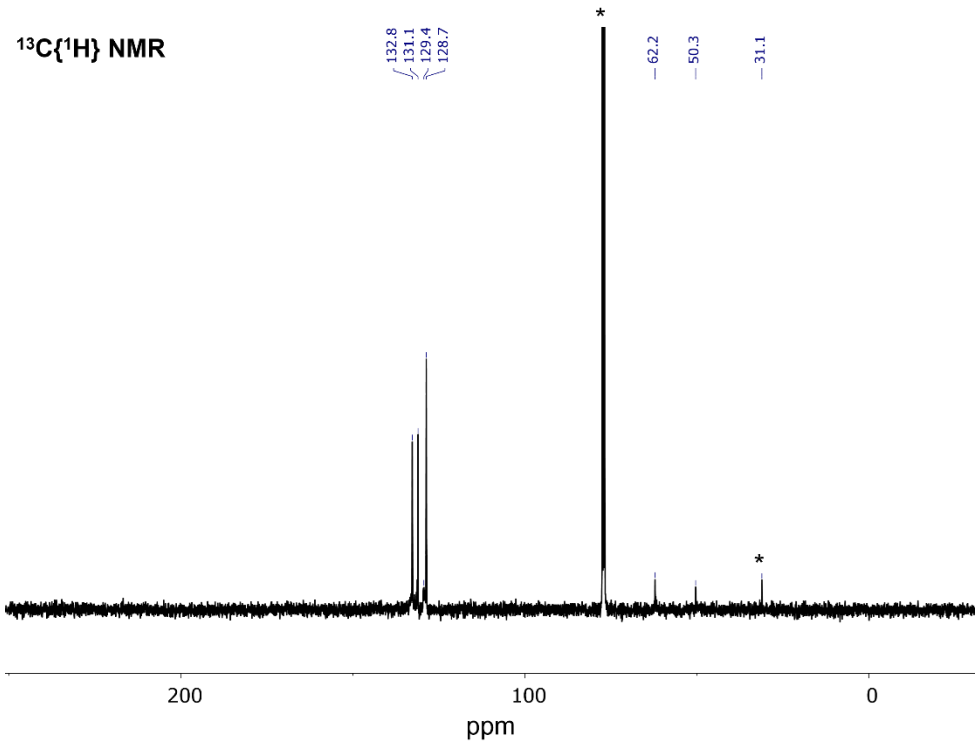

Figure S24: High resolution ES-MS spectrum for **ReO_2-NP_2Me** (**Re-6**)

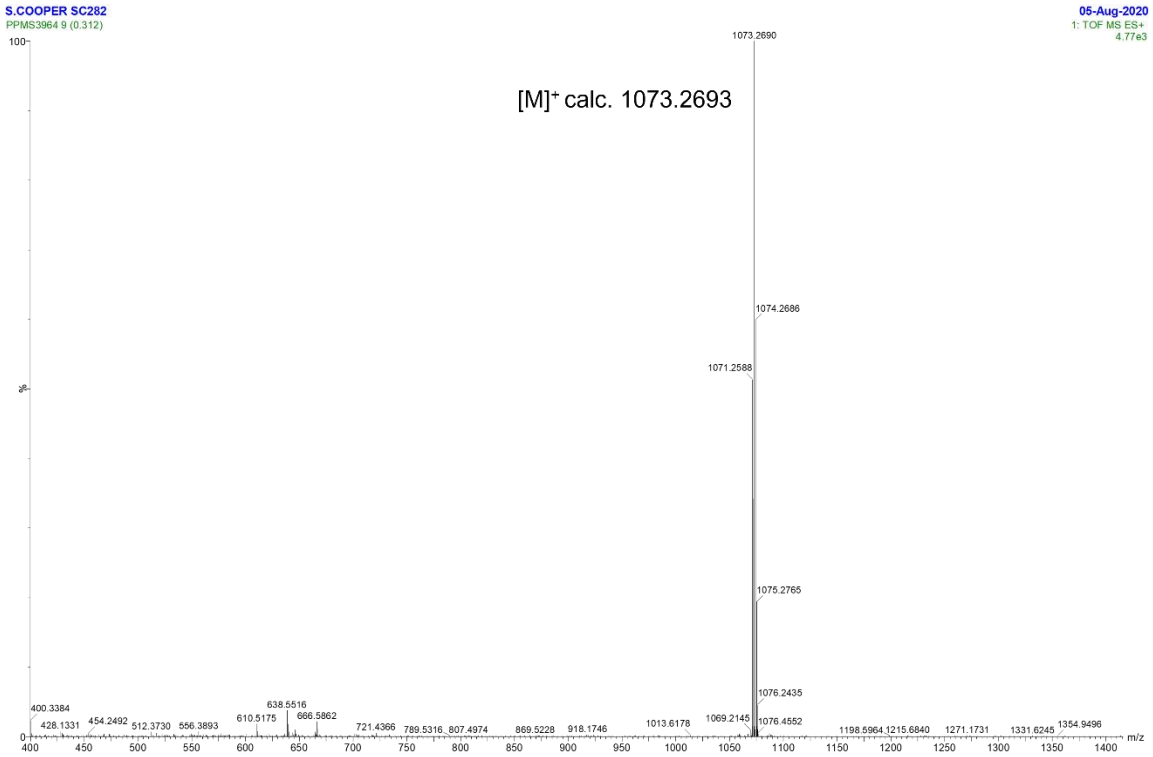

Figure S25: ^{1}H NMR spectrum (d^{3}-MeOD, 400 MHz, 298 K) of **ReO_2-NP_2Et** (**Re-7**). Asterisks indicate solvent impurities.

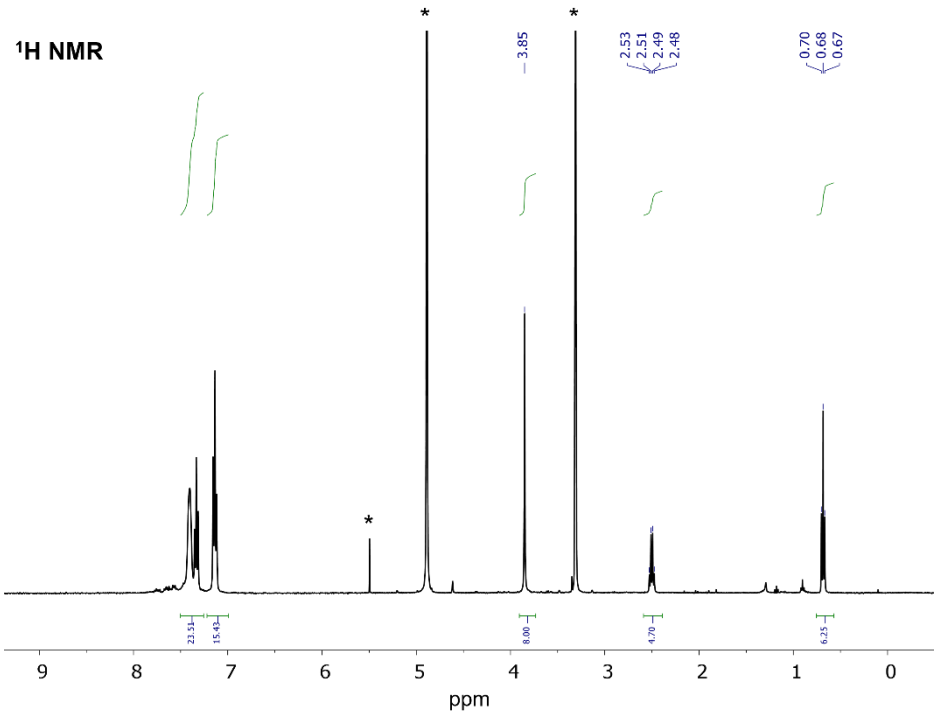

Figure S26: ^{31}P{^{1}H} NMR spectrum (d^{3}-MeOD, 400 MHz, 298 K) of **ReO_2-NP_2Et** (**Re-7**).

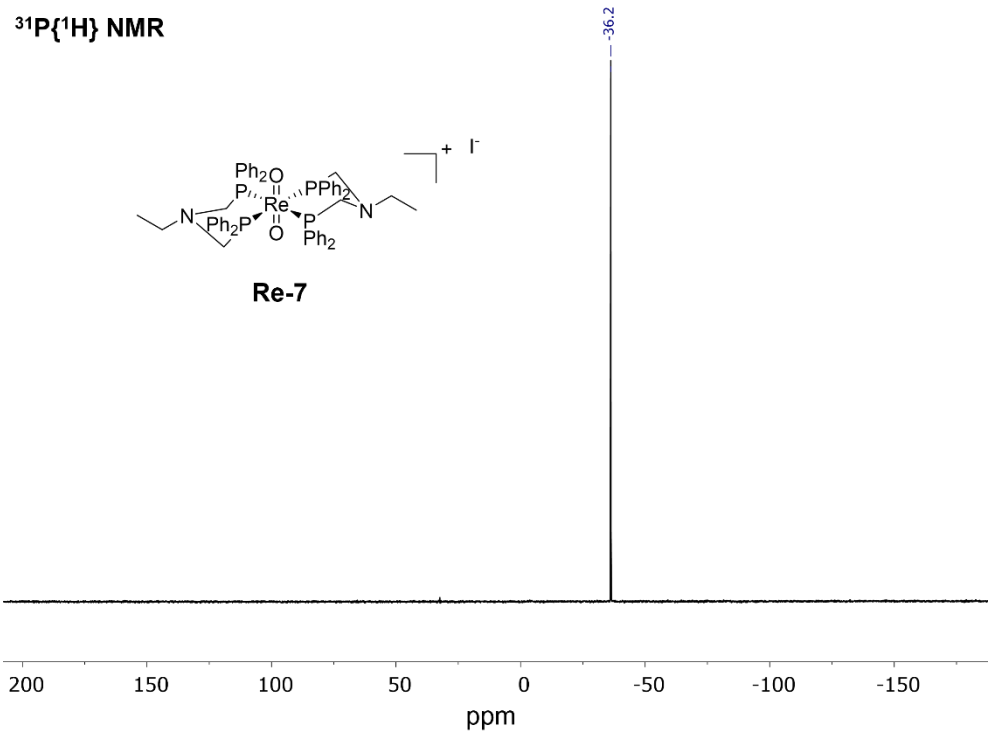

Figure S27: $^{13}C\{^{1}H\}$ NMR spectrum ($CDCl_3$, 400 MHz, 298 K) of **ReO_2-NP_2Et** (**Re-7**). Asterisks indicate solvent impurities.

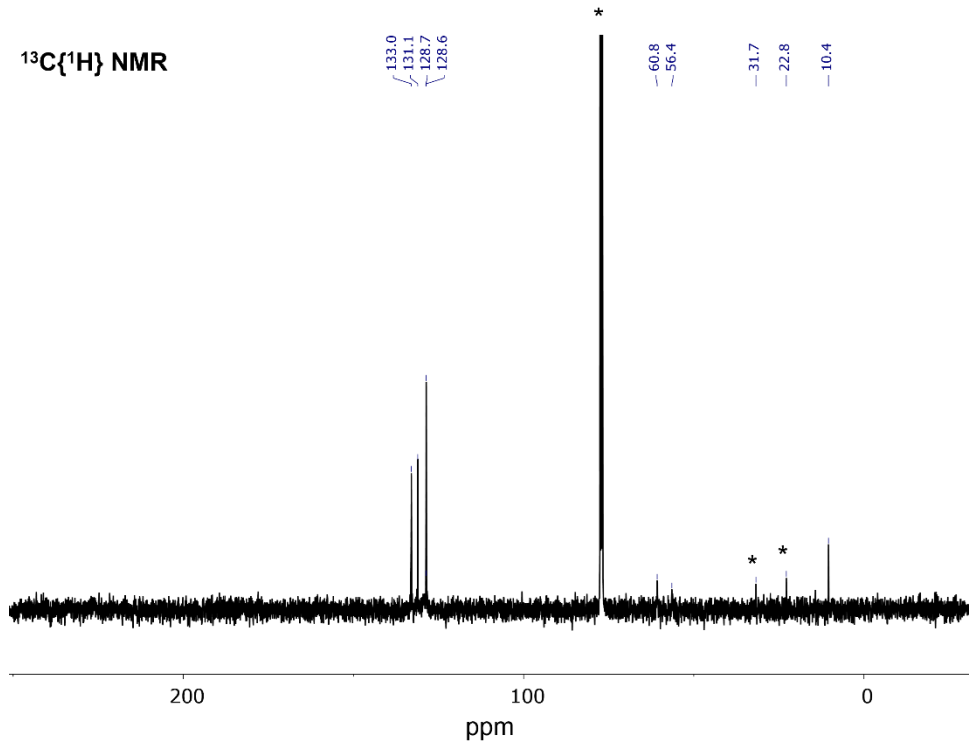

Figure S28: High resolution ES-MS spectrum for **ReO_2-NP_2Et** (**Re-7**)

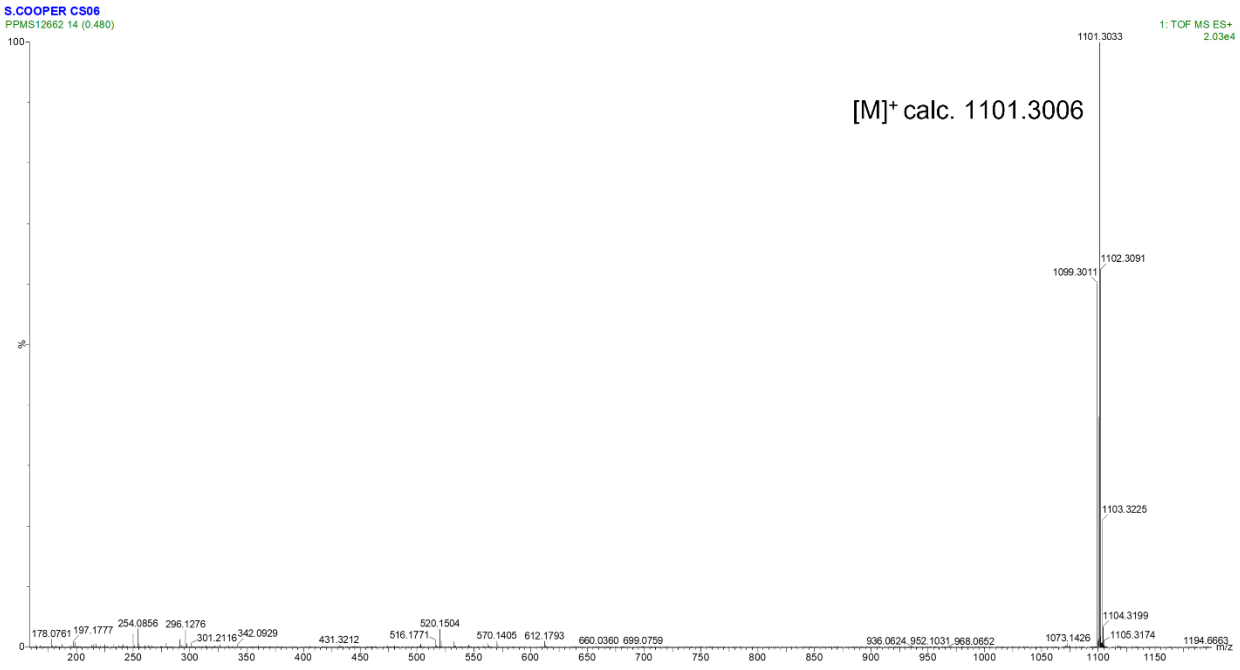

Figure S29: ^{1}H NMR spectrum ($CDCl_3$, 400 MHz, 298 K) of **ReO_2-NP_2iPr** (**Re-8**). Asterisks indicate solvent impurities.

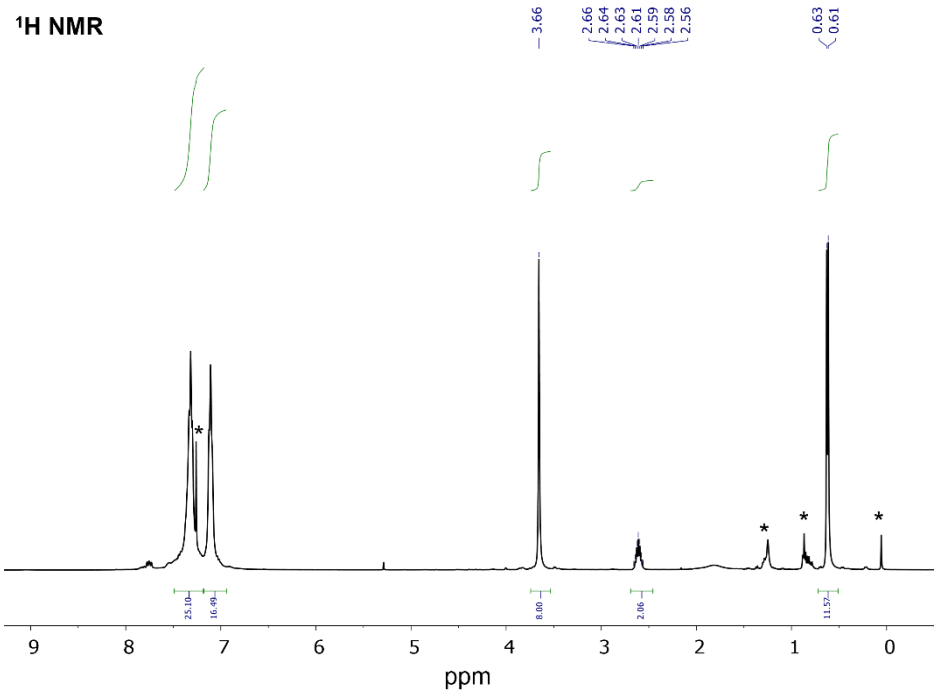

Figure S30: $^{31}P\{^{1}H\}$ NMR spectrum ($CDCl_3$, 400 MHz, 298 K) of **ReO_2-NP_2iPr** (**Re-8**).

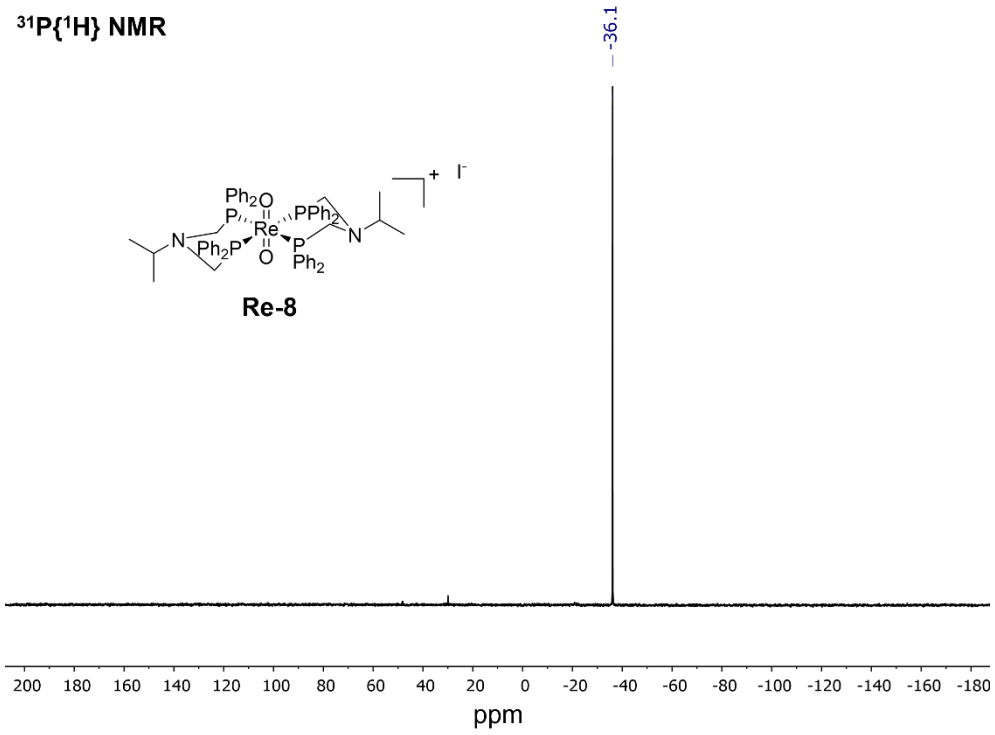

Figure S31: $^{13}C\{^{1}H\}$ NMR spectrum ($CDCl_3$, 400 MHz, 298 K) of **ReO_2-NP_2iPr** (**Re-8**). Asterisks indicate solvent impurities.

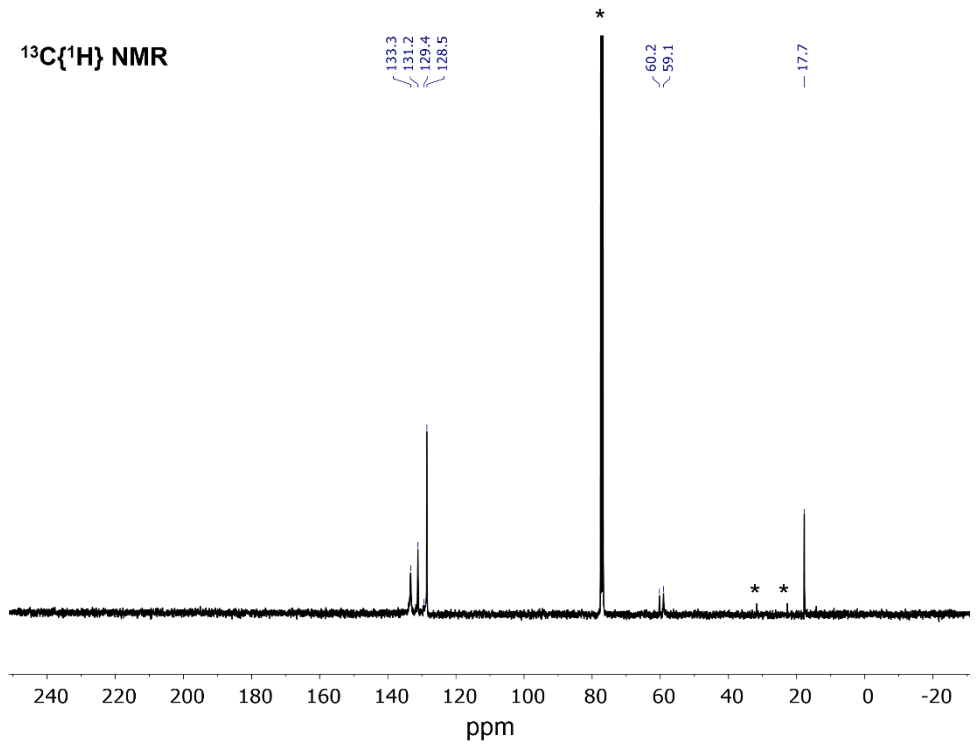

Figure S32: High resolution ES-MS spectrum for **ReO_2-NP_2iPr** (**Re-8**)

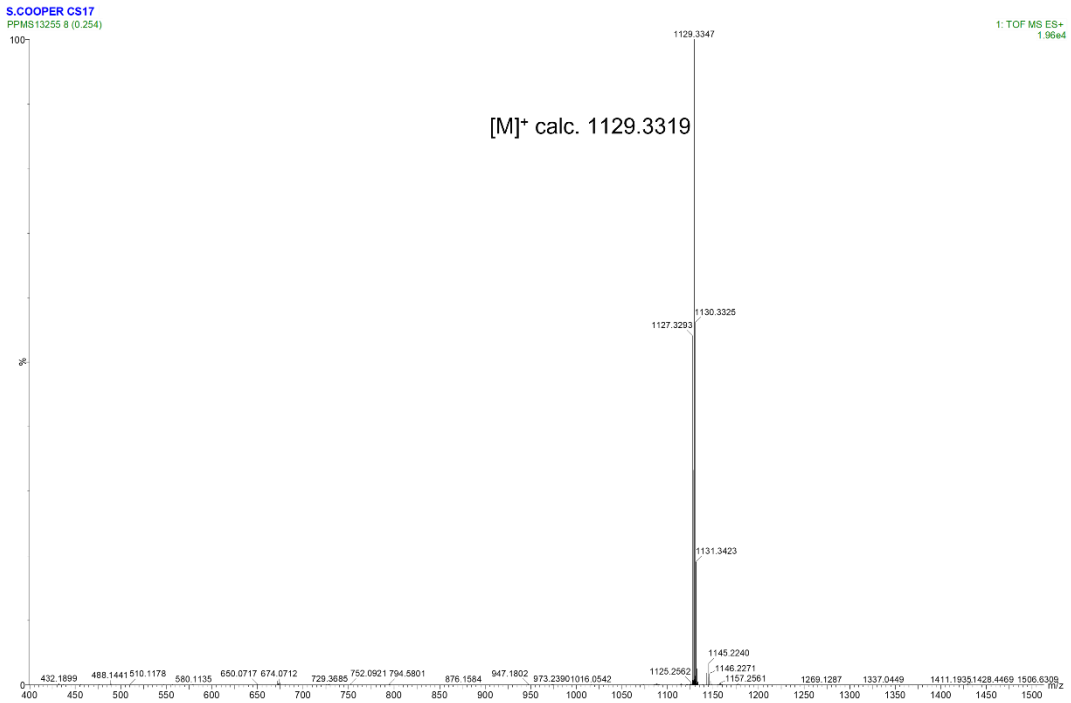

Figure S33: ^{1}H NMR spectrum ($CDCl_3$, 400 MHz, 298 K) of **ReO_2-NP_2tBu** (**Re-9**). Asterisks indicate solvent impurities.

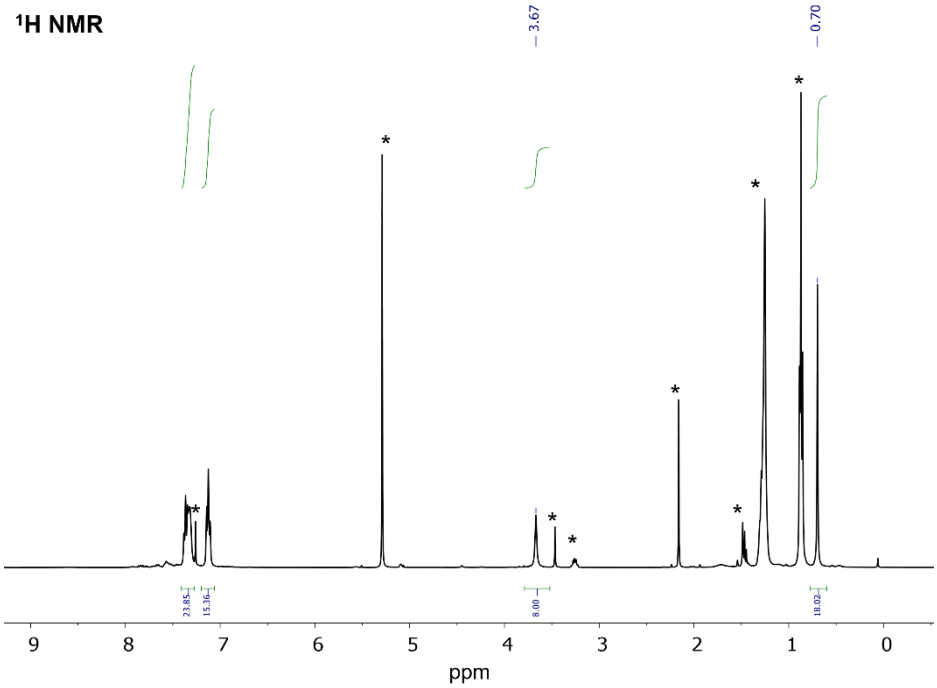

Figure S34: ^{31}P{^{1}H} NMR spectrum ($CDCl_3$, 400 MHz, 298 K) of **ReO_2-NP_2tBu** (**Re-9**).

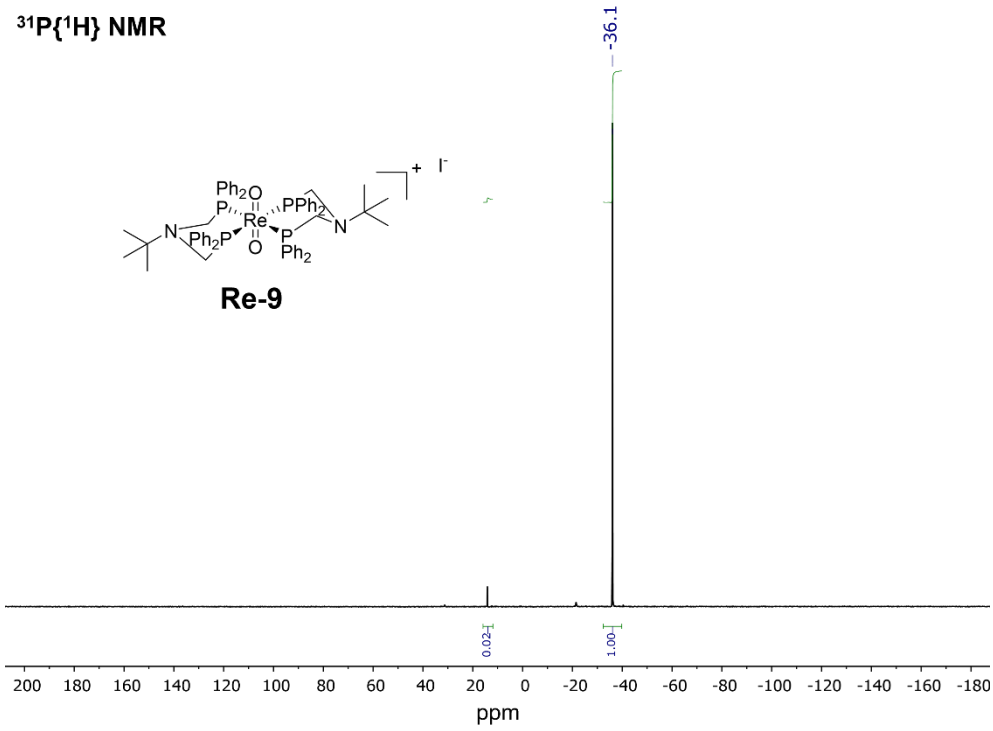

Figure S35: $^{13}C\{^{1}H\}$ NMR spectrum ($CDCl_3$, 400 MHz, 298 K) of **ReO_2-NP_2tBu** (**Re-9**). Asterisks indicate solvent impurities.

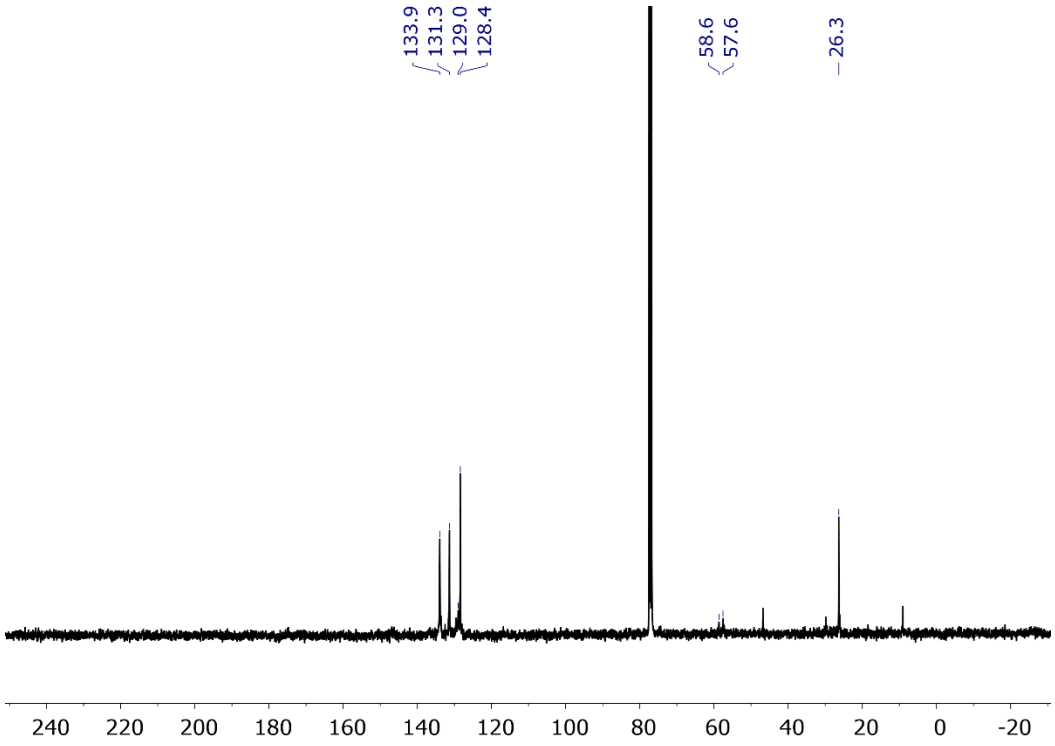

Figure S36: High resolution ES-MS spectrum for **ReO_2-NP_2tBu** (**Re-9**)

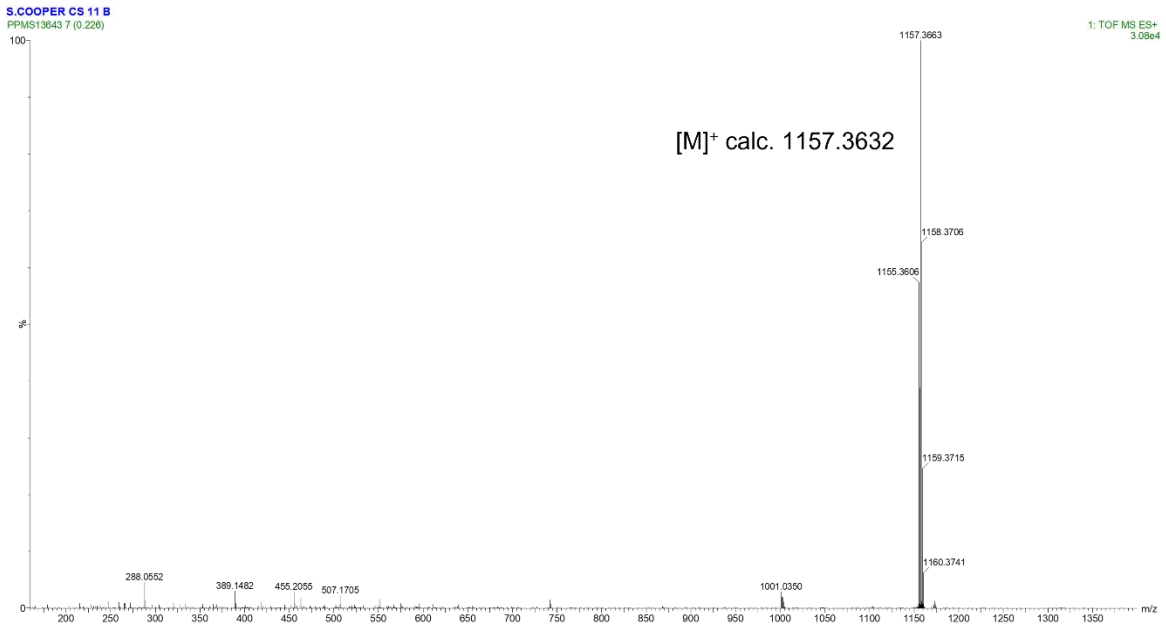

Figure S37: ^{1}H NMR spectrum ($CDCl_3$, 400 MHz, 298 K) of **ReO_2-NP_2Cyh** (**Re-10**). Asterisks indicate solvent impurities.

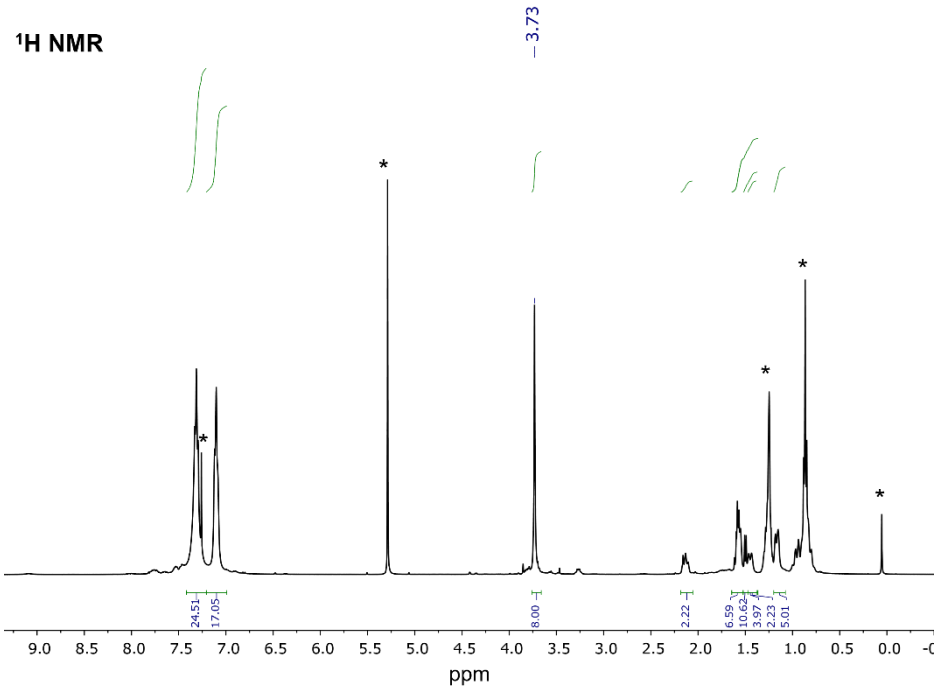

Figure S38: ^{31}P{^{1}H} NMR spectrum ($CDCl_3$, 400 MHz, 298 K) of **ReO_2-NP_2Cyh** (**Re-10**).

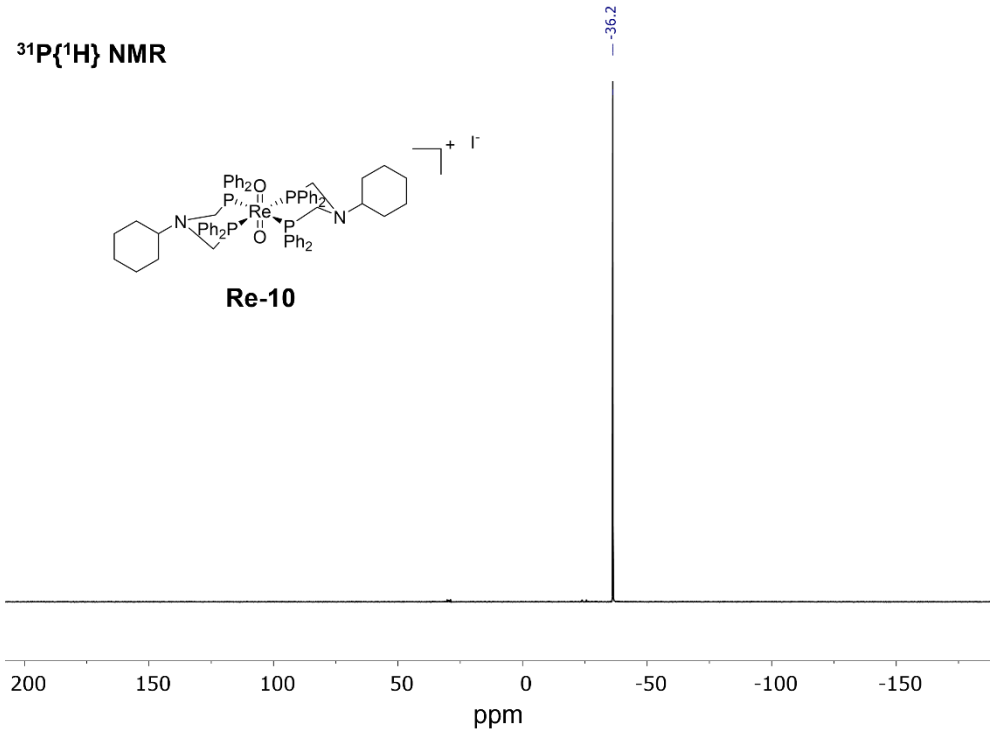

Figure S39: $^{13}C\{^{1}H\}$ NMR spectrum ($CDCl_3$, 400 MHz, 298 K) of **ReO_2-NP_2Cyh** (**Re-10**). Asterisks indicate solvent impurities.

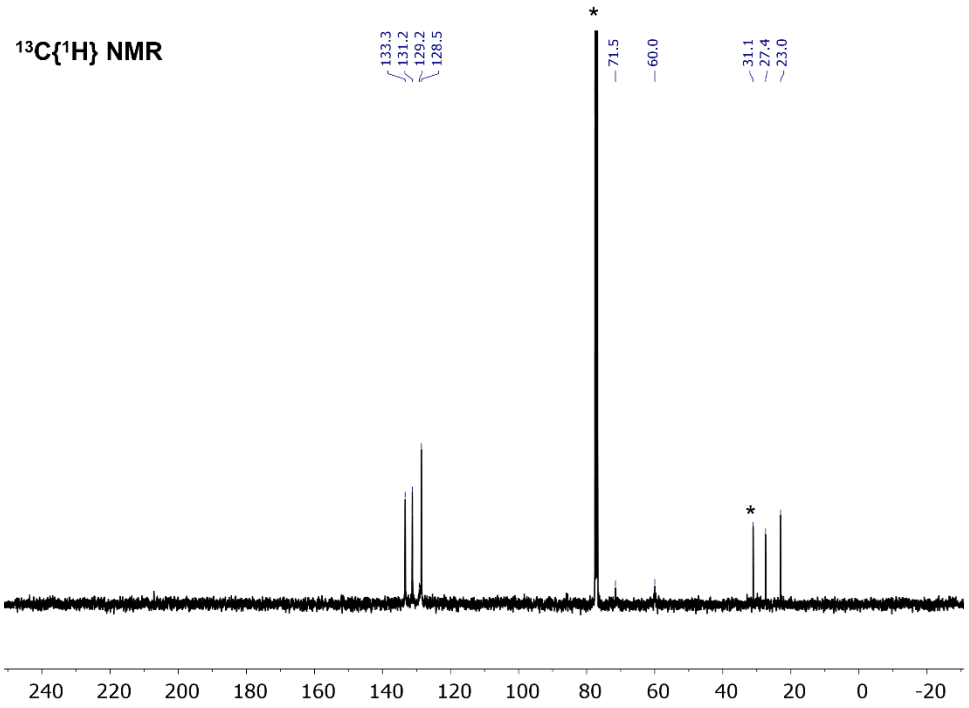

Figure S40: High resolution ES-MS spectrum for **ReO_2-NP_2Cyh** (**Re-10**)

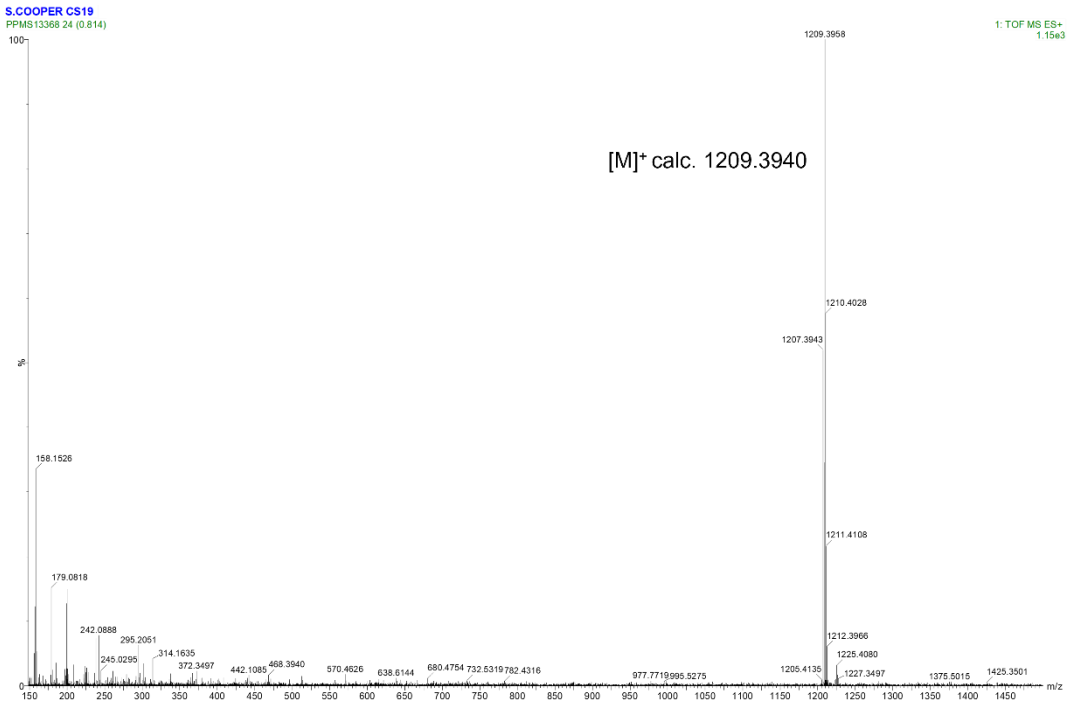

Figure S41: ^{1}H NMR spectrum ($CDCl_3$, 400 MHz, 298 K) of **ReO_2-NP_2Cyp** (**Re-11**). Asterisks indicate solvent impurities.

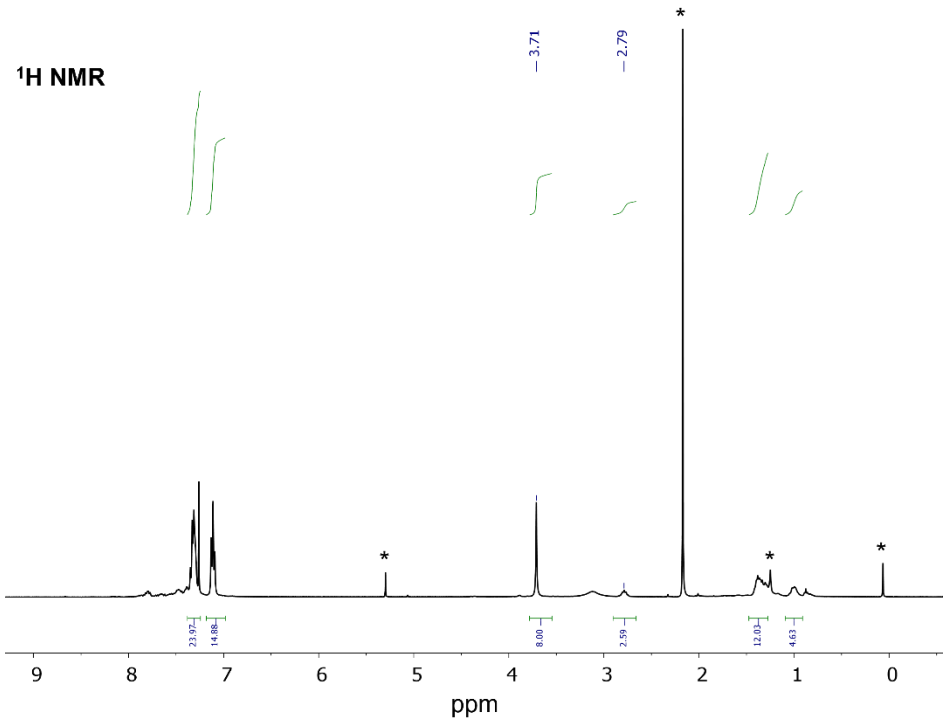

Figure S42: $^{31}P\{^{1}H\}$ NMR spectrum ($CDCl_3$, 400 MHz, 298 K) of **ReO_2-NP_2Cyp** (**Re-11**).

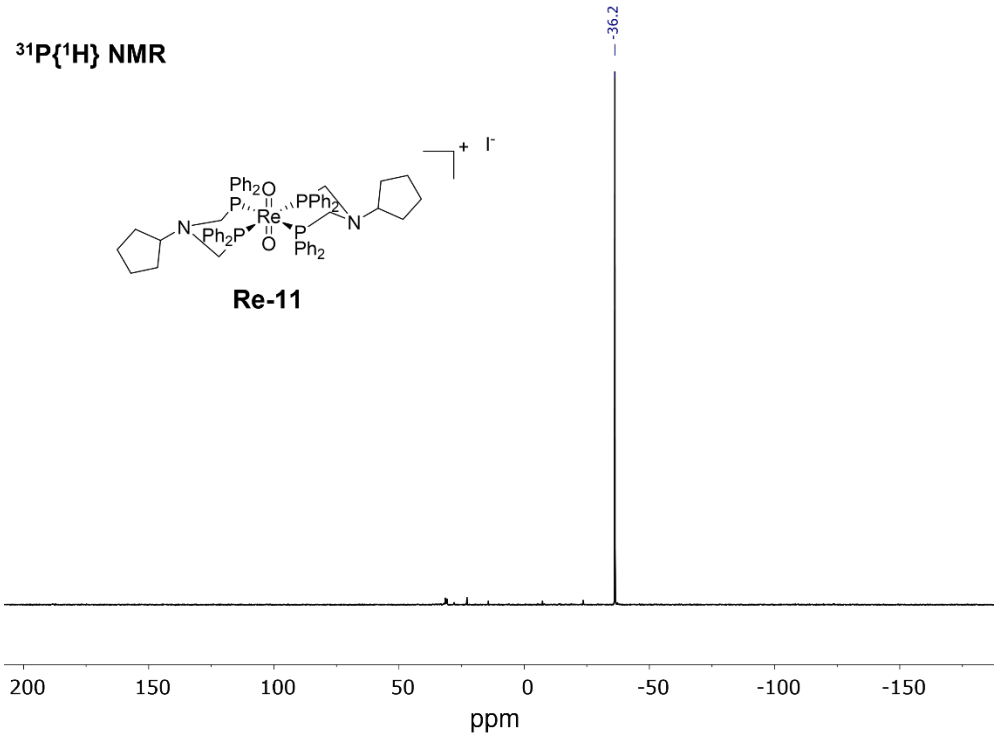

Figure S43: $^{13}C\{^{1}H\}$ NMR spectrum ($CDCl_3$, 400 MHz, 298 K) of **ReO_2-NP_2Cyp** (**Re-11**). Asterisks indicate solvent impurities.

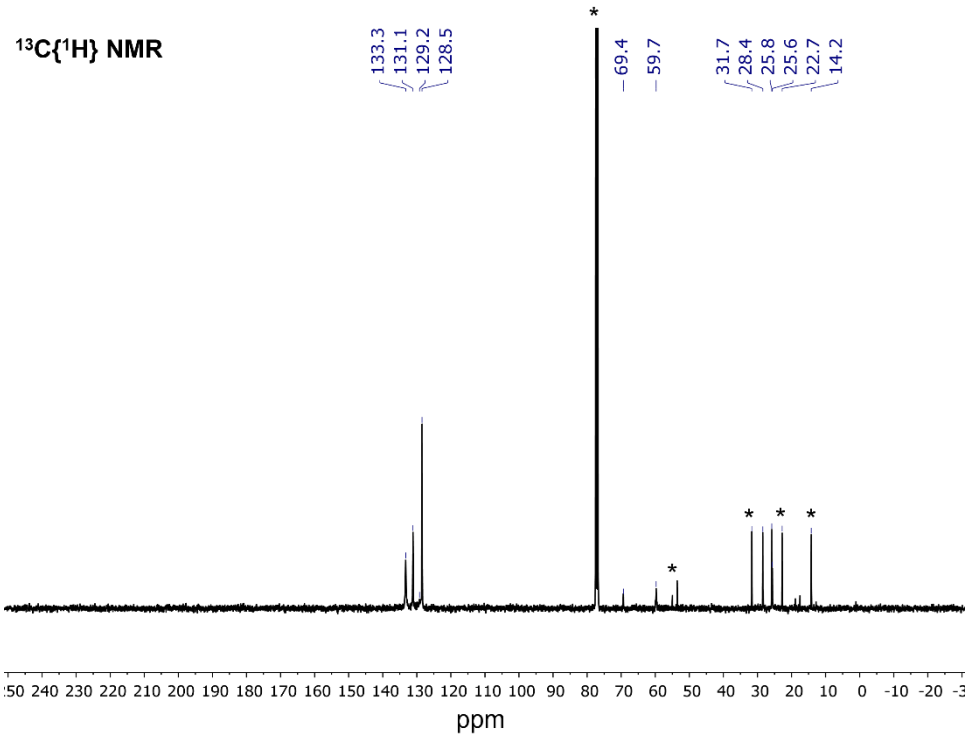

Figure S44: High resolution ES-MS spectrum for **ReO_2-NP_2Cyp** (**Re-11**)

Figure S45: ^{1}H NMR spectrum ($CDCl_3$, 400 MHz, 298 K) of **ReO_2-NP_2Cypr** (**Re-12**). Asterisks indicate solvent impurities.

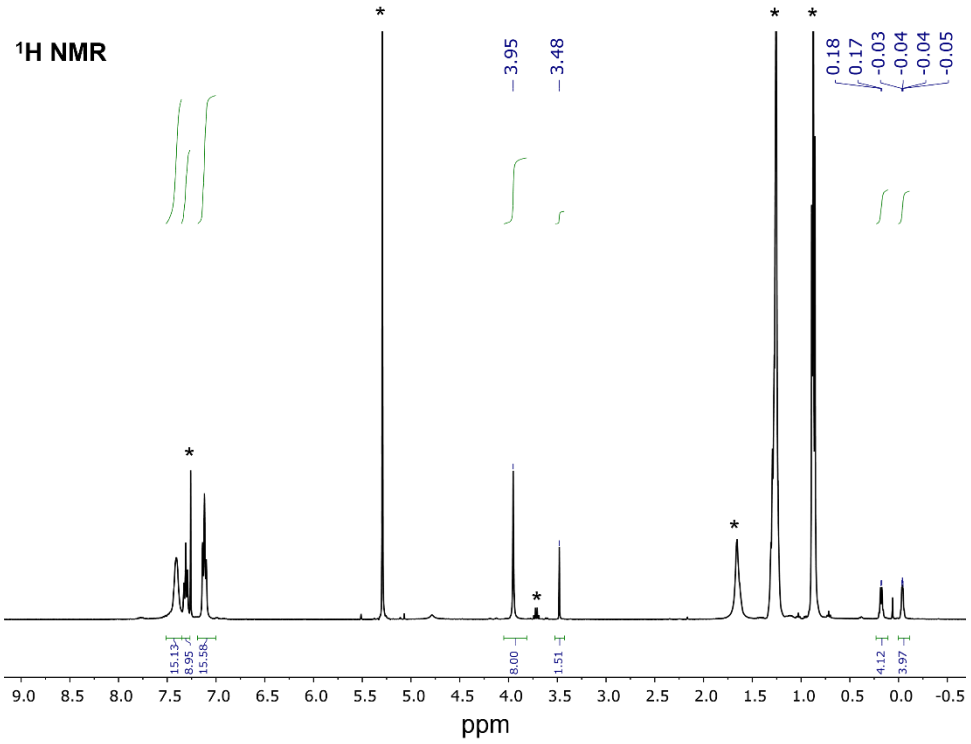

Figure S46: $^{31}P\{^{1}H\}$ NMR spectrum ($CDCl_3$, 400 MHz, 298 K) of **ReO_2-NP_2Cypr** (**Re-12**).

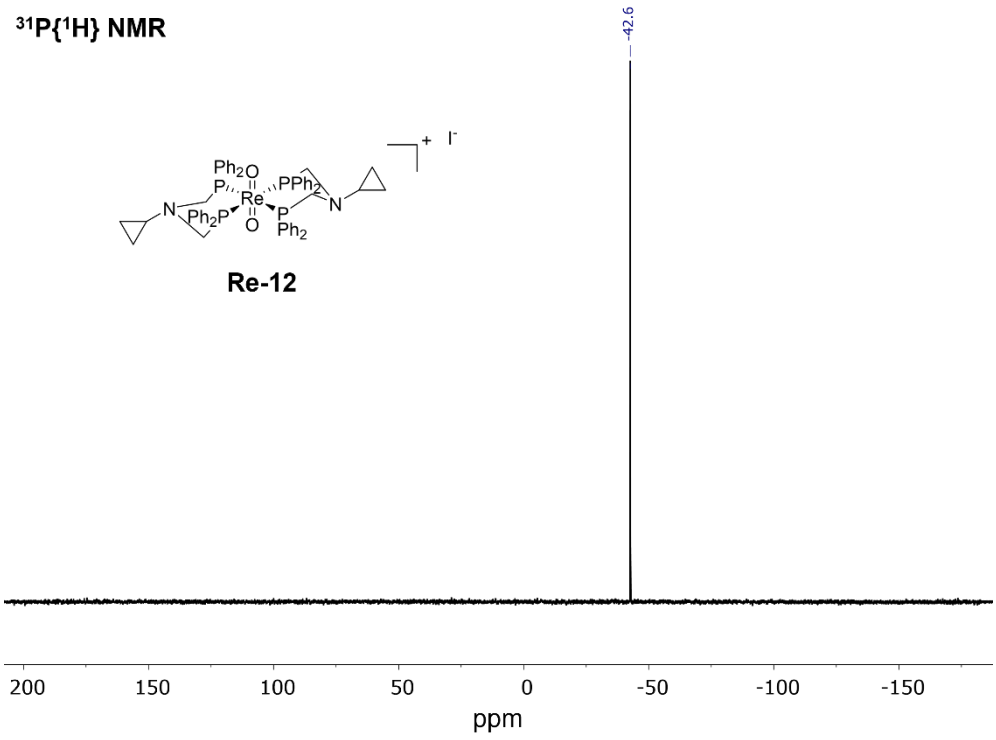

Figure S47: $^{13}C\{^{1}H\}$ NMR spectrum ($CDCl_3$, 400 MHz, 298 K) of **ReO_2-NP_2Cypr** (**Re-12**). Asterisks indicate solvent impurities.

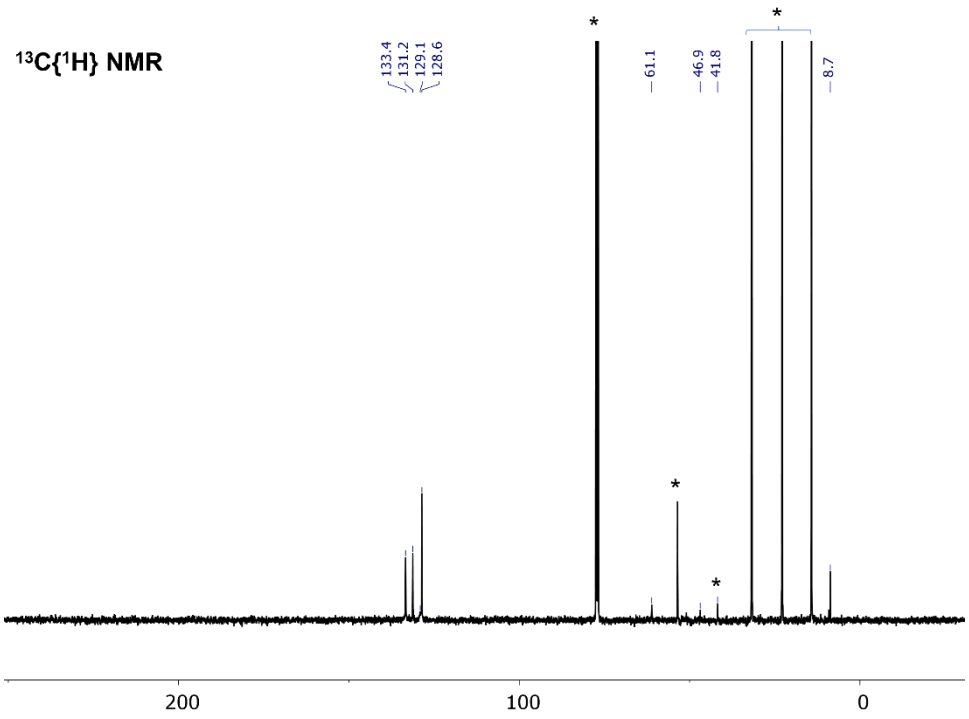

Figure S48: High resolution ES-MS spectrum for **ReO_2-NP_2Cypr** (**Re-12**)

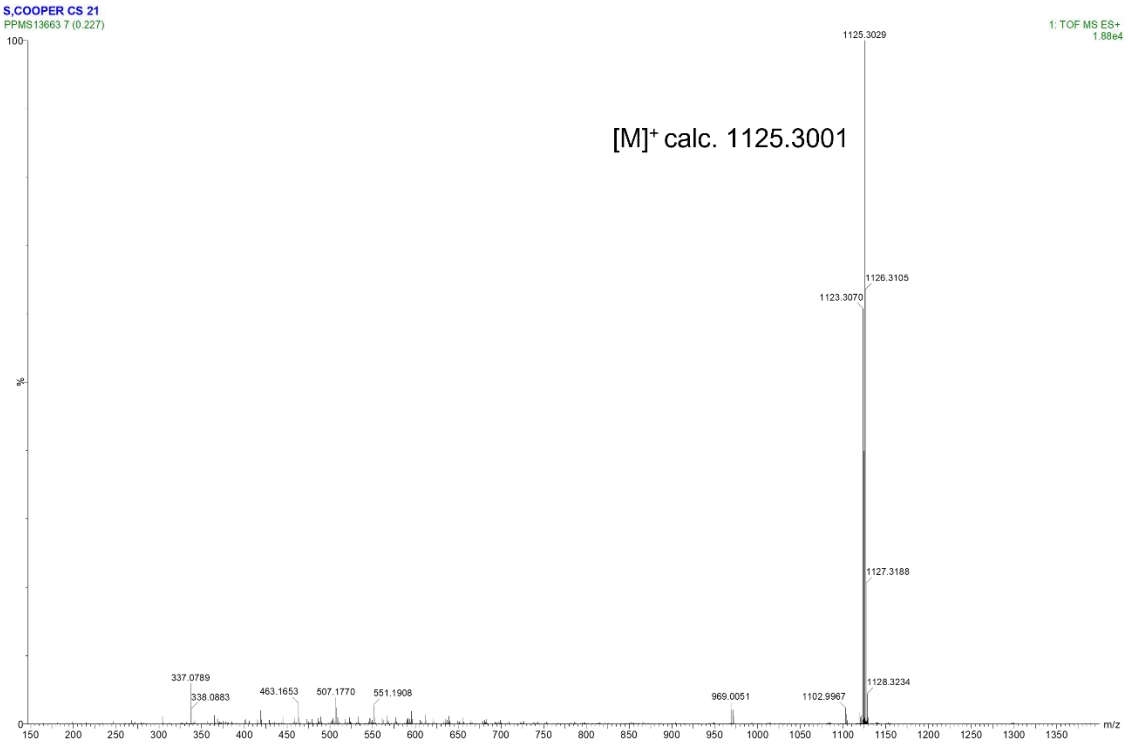

Figure S49: ^{1}H NMR spectrum ($CDCl_3$, 400 MHz, 298 K) of **ReO_2-NP_2Bn** (**Re-13**). Asterisks indicate solvent impurities.

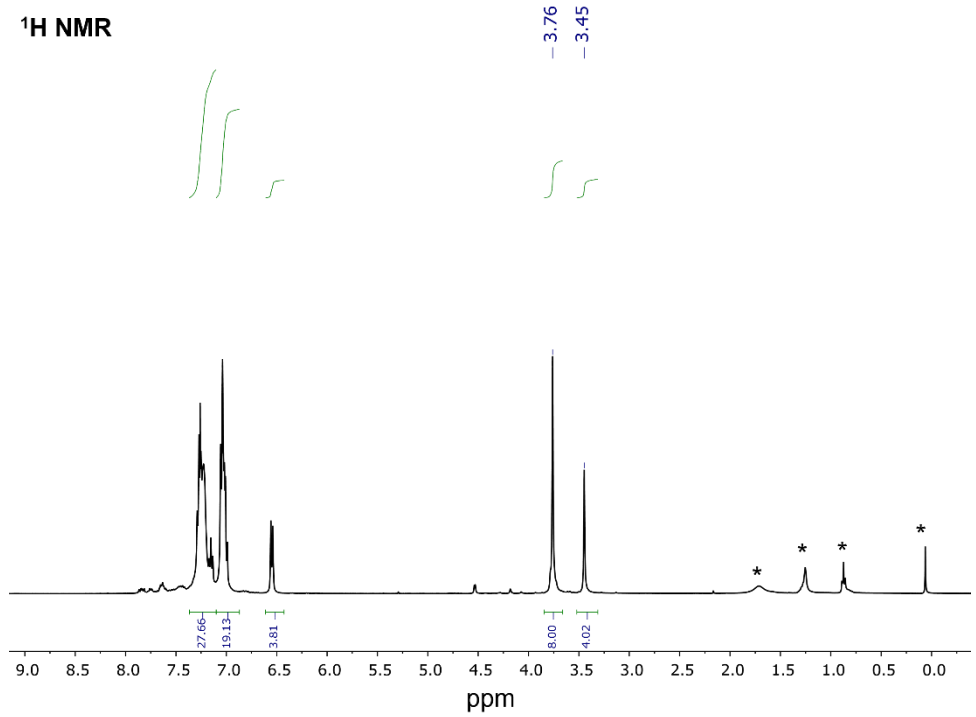

Figure S50: ^{31}P{^{1}H} NMR spectrum ($CDCl_3$, 400 MHz, 298 K) of **ReO_2-NP_2Bn** (**Re-13**).

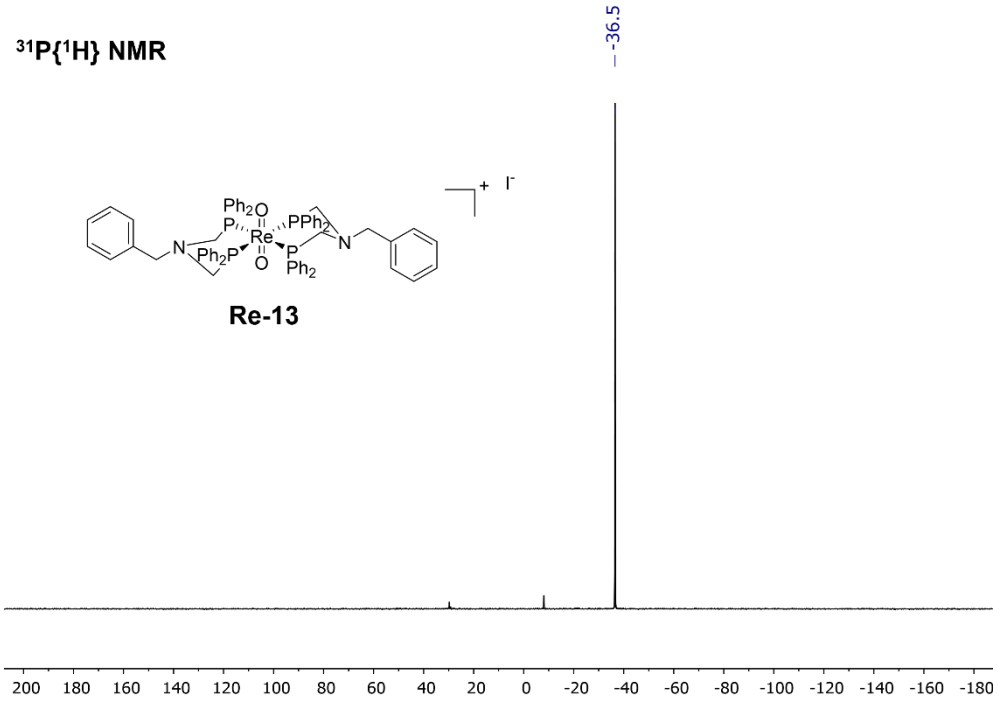

Figure S51: $^{13}C\{^{1}H\}$ NMR spectrum ($CDCl_3$, 400 MHz, 298 K) of **ReO_2-NP_2Bn** (**Re-13**). Asterisks indicate solvent impurities.

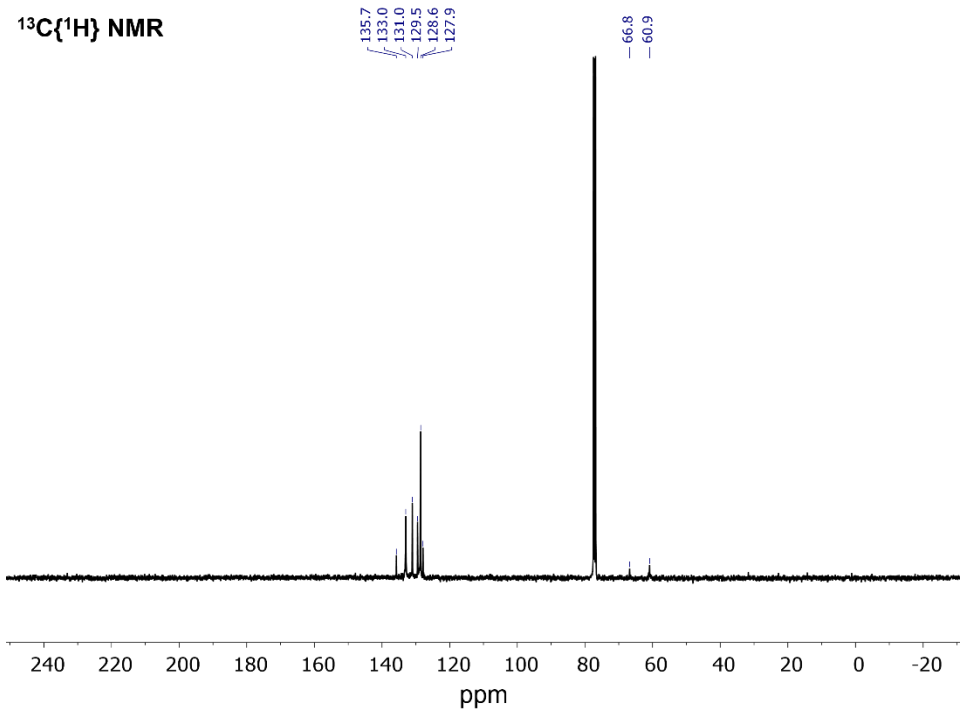

Figure S52: High resolution ES-MS spectrum for **ReO_2-NP_2Bn** (**Re-13**)

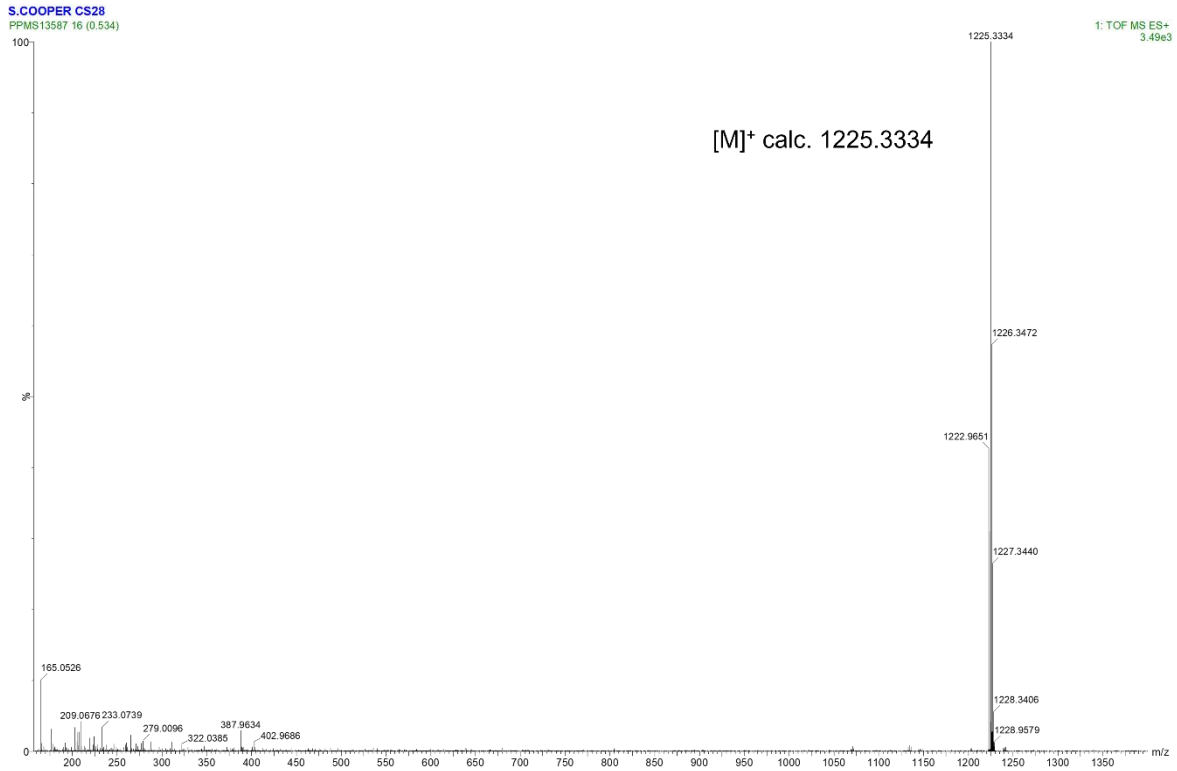

Figure S53: ^{1}H NMR spectrum ($CDCl_3$, 400 MHz, 298 K) of **ReO_2-NP_2Bn** (**Re-13**). Asterisks indicate solvent impurities.

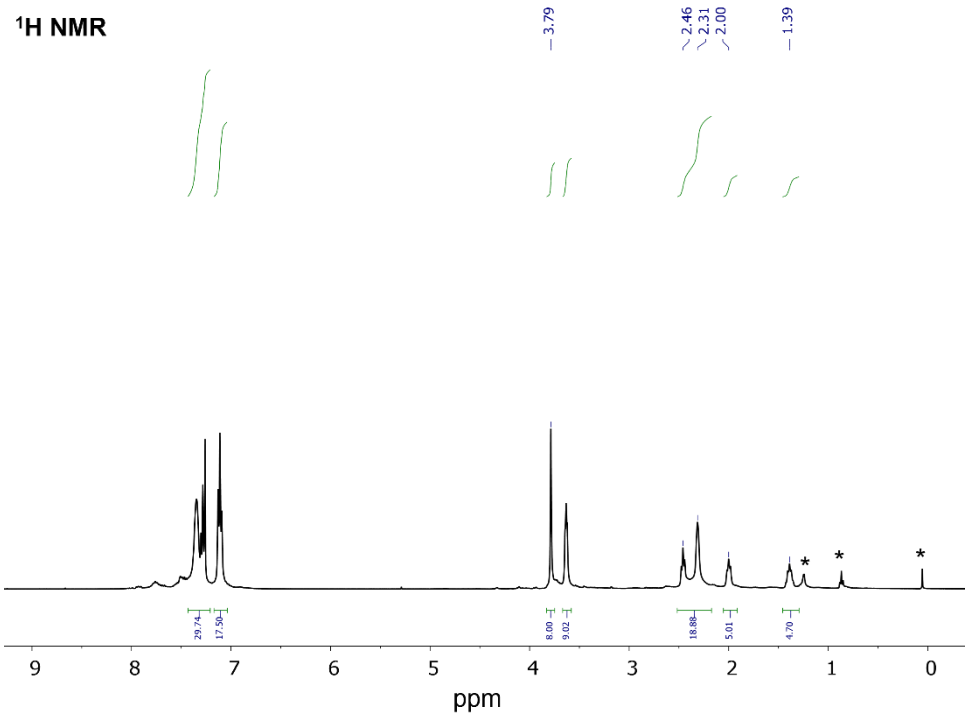

Figure S54: ^{31}P{^{1}H} NMR spectrum ($CDCl_3$, 400 MHz, 298 K) of **ReO_2-NP_2Bn** (**Re-13**).

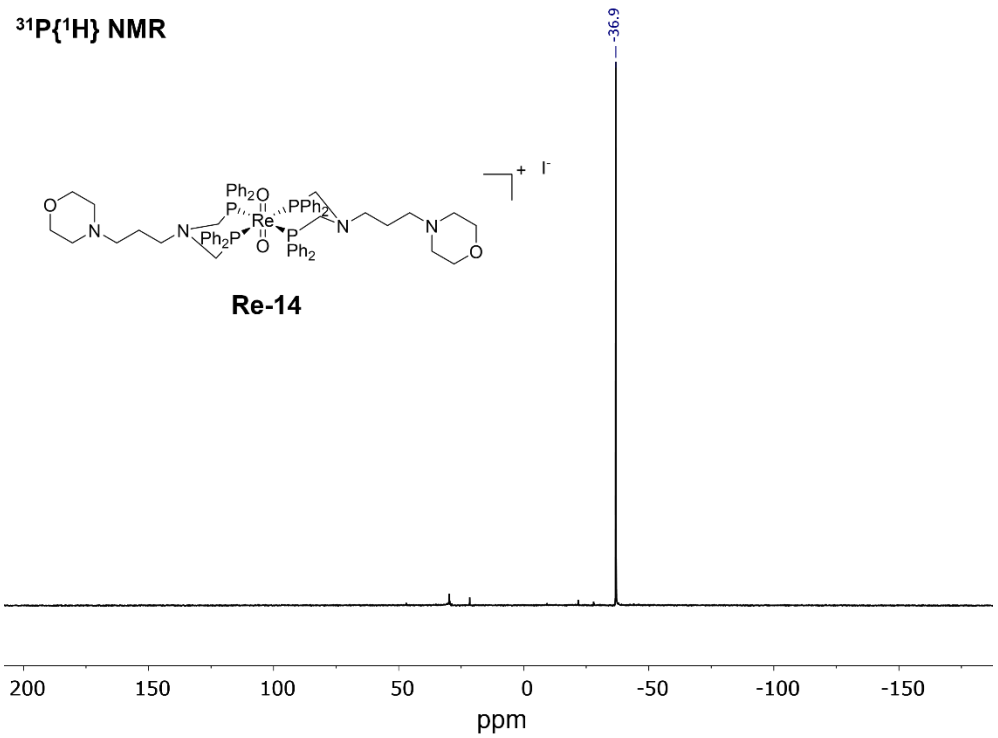

Figure S55: $^{13}C\{^{1}H\}$ NMR spectrum ($CDCl_3$, 400 MHz, 298 K) of **ReO_2-NP_2Bn** (**Re-13**). Asterisks indicate solvent impurities.

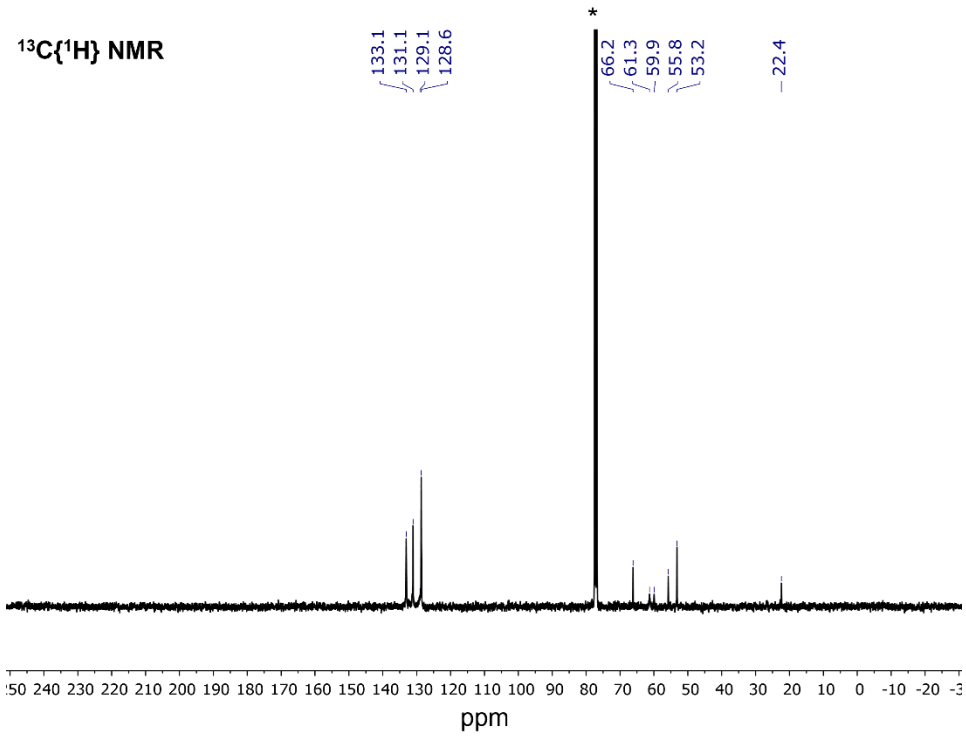

Figure S56: High resolution ES-MS spectrum for **ReO_2-NP_2Mor** (**Re-14**)

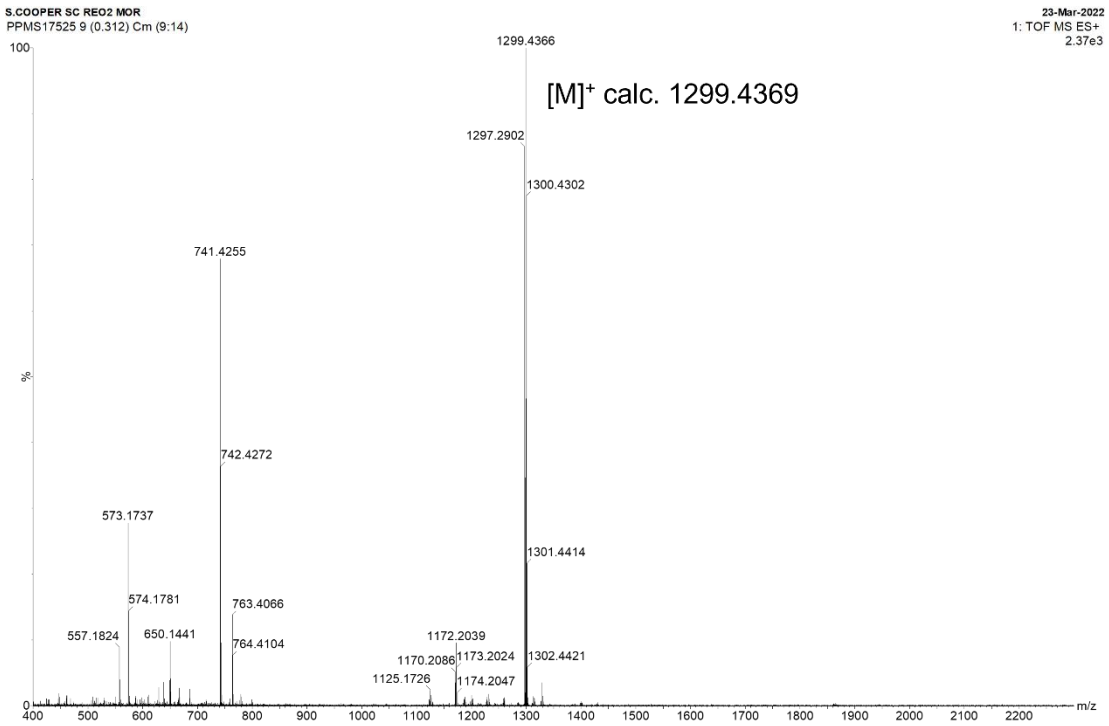

S5) X-ray Crystallography

The X-ray crystal structure of Re-1

Crystal data for **Re-1**: $[C_{64}H_{58}N_2O_4P_4Re](I)\cdot 4.5(C_6H_{14})$, M = 1743.87, trigonal, R-3 (no. 148), a = 30.4077(5), b = 30.4077(5), c = 23.4090(4) Å, V = 18744.8(8) Å^3, Z = 9 [C_i symmetry], D_c = 1.390 g cm^{-3}, μ(Mo-Kα) = 1.957 mm^{-1}, T = 173 K, orange/brown blocks, Agilent Xcalibur 3 E diffractometer; 8249 independent measured reflections (R_{int} = 0.0210), F^2 refinement,[8,9] R_1(obs) = 0.0288, wR_2(all) = 0.0803, 6695 independent observed absorption-corrected reflections [$|F_o| > 4\sigma(|F_o|)$, completeness to θ_{full}(25.2°) = 98.8%], 347 parameters. CCDC 2165137.

The rhenium complex in the structure of **Re-1** was found to sit across a centre of symmetry at the metal atom. The N1-bound –C_6H_4OH group was found to be disordered, and two orientations were identified of *ca*. 57 and 43% occupancy, approximately corresponding to a 180° rotation about the N1–C6 vector (*i.e.* flipping the position of the OH group). The geometries of the two orientations were optimised, the thermal parameters of adjacent atoms were restrained to be similar, and only the non-hydrogen atoms of the major occupancy orientation were refined anisotropically (those of the minor occupancy orientation were refined isotropically). The O–H hydrogen atom could not be located for either partial-occupancy orientation, and so they were added in idealised positions with O–H distances of 0.90 Å and allowed to rotate about the C–O vector to find the best fit with the observed electron density (the SHELX HFIX/AFIX 147 command). Both the iodide anion and the included solvent were found to be highly disordered, and the best approach to handling this diffuse electron density was found to be the SQUEEZE routine of PLATON.[10] This suggested a total of 2495 electrons per unit cell, equivalent to 277.2 electrons per complex. The iodide anion accounts for 53 of these electrons, leaving 224.2 electrons for the solvent. Before the use of SQUEEZE the solvent most resembled hexane (C_6H_{14}, 50 electrons), and 4.5 dichloromethane molecules corresponds to 225 electrons, so this was used as the solvent present. As a result, the atom list for the asymmetric unit is low by 0.5 x [I + 4.5(C_6H_{14})] = $C_{13.5}H_{31.5}I_{0.5}$ (and that for the unit cell low by $C_{243}H_{567}I_9$) compared to what is actually presumed to be present.

The X-ray crystal structure of Re-3

Crystal data for **Re-3**: $[C_{68}H_{62}N_2O_6P_4Re](I)\cdot 1.75(CH_2Cl_2)$, M = 1588.79, trigonal, R-3 (no. 148), a = 29.5291(7), b = 29.5291(7), c = 24.5448(5) Å, V = 18534.9(9) Å^3, Z = 9 [C_i symmetry], D_c = 1.281 g cm^{-3}, μ(Mo-Kα) = 1.281 mm^{-1}, T = 173 K, yellow blocks, Agilent Xcalibur 3 E diffractometer; 8080 independent measured reflections (R_{int} = 0.0181), F^2 refinement,[8,9] R_1(obs) = 0.0463, wR_2(all) = 0.1510, 6755 independent observed absorption-corrected

reflections [$|F_o| > 4\sigma(|F_o|)$, completeness to $\theta_{full}(25.2°)$ = 98.1%], 419 parameters. CCDC 2165138.

The rhenium complex in the structure of **Re-3** was found to sit across a centre of symmetry at the metal atom. The N1-bound $–C_6H_4CH_2COOH$ group was found to be disordered. Two orientations were identified of *ca*. 63 and 37% occupancy, their geometries were optimised, the thermal parameters of adjacent atoms were restrained to be similar, and only the non-hydrogen atoms of the major occupancy orientation were refined anisotropically (those of the minor occupancy orientation were refined isotropically). The –COOH hydrogen atom could not be located for either partial-occupancy orientation, and so they were added in idealised positions with O–H distances of 0.90 Å and allowed to rotate about the C–O vector to find the best fit with the observed electron density (the SHELX HFIX/AFIX 147 command). However, the positions of these hydrogens atoms never settled and so they were fixed in arbitrary positions to allow for a converged refinement. The iodide anion was found to be distributed across four sites one of which was disordered over three positions. For this disordered site the thermal parameters of the three atoms were restrained to be similar. The included solvent was found to be highly disordered, and the best approach to handling this diffuse electron density was found to be the SQUEEZE routine of PLATON.[10] This suggested a total of 670 electrons per unit cell, equivalent to 74.4 electrons per complex. Before the use of SQUEEZE the solvent was unclear, and so the most recently used solvent [dichloromethane (CH_2Cl_2, 42 electrons)] was assumed. 1.75 dichloromethane molecules corresponds to 73.5 electrons, so this was used as the solvent present. As a result, the atom list for the asymmetric unit is low by 0.5 x 1.75(CH_2Cl) = $C_{0.875}H_{1.75}Cl_{1.75}$ (and that for the unit cell low by $C_{15.75}H_{31.5}Cl_{31.5}$) compared to what is actually presumed to be present

The X-ray crystal structure of Re-4

Crystal data for **Re-4**: $[C_{54}H_{56}N_2O_8P_6Re](Cl)\cdot 2(C_6H_{14})$, M = 1440.82, triclinic, P-1 (no. 2), a = 12.9710(3), b = 14.1823(3), c = 18.7894(3) Å, α = 91.9605(16), β = 101.2884(16), γ = 114.1629(19)°, V = 3067.26(11) Å^3, Z = 2 [two independent C_i symmetric complexes], D_c = 1.560 g cm^{-3}, μ(Mo-Kα) = 2.240 mm^{-1}, T = 173 K, pale yellow blocks, Agilent Xcalibur 3 E diffractometer; 13231 independent measured reflections (R_{int} = 0.0333), F^2 refinement,[8,9] R_1(obs) = 0.0366, wR_2(all) = 0.0761, 10719 independent observed absorption-corrected reflections [$|F_o| > 4\sigma(|F_o|)$, completeness to $\theta_{full}(25.2°)$ = 99.8%], 643 parameters. CCDC 2165139.

The structure of **Re-4** was found to contain two crystallographically independent complexes (**Re-4-A** and **Re-4-B**) in the asymmetric unit, each of which sits across a centre of symmetry at the rhenium atom. The presumed two OH hydrogen atoms of the P7-based PO_3

unit of each independent molecule could not be reliably located and were omitted, making the atom list 4H low.

Both the chloride anion and the included solvent were found to be highly disordered, and the best approach to handling this diffuse electron density was found to be the SQUEEZE routine of PLATON.[10] This suggested a total of 240 electrons per unit cell, equivalent to 120 electrons per complex. The chloride anion accounts for 17 of these electrons, leaving 103 electrons for the solvent. Before the use of SQUEEZE the solvent most resembled hexane (C_6H_{14}, 50 electrons), and 2 dichloromethane molecules corresponds to 100 electrons, so this was used as the solvent present. As a result, the atom list for the asymmetric unit is low by 4H + Cl + 2(C_6H_{14})] = $C_{12}H_{32}Cl$ (and that for the unit cell low by $C_{24}H_{64}Cl_2$) compared to what is actually presumed to be present.

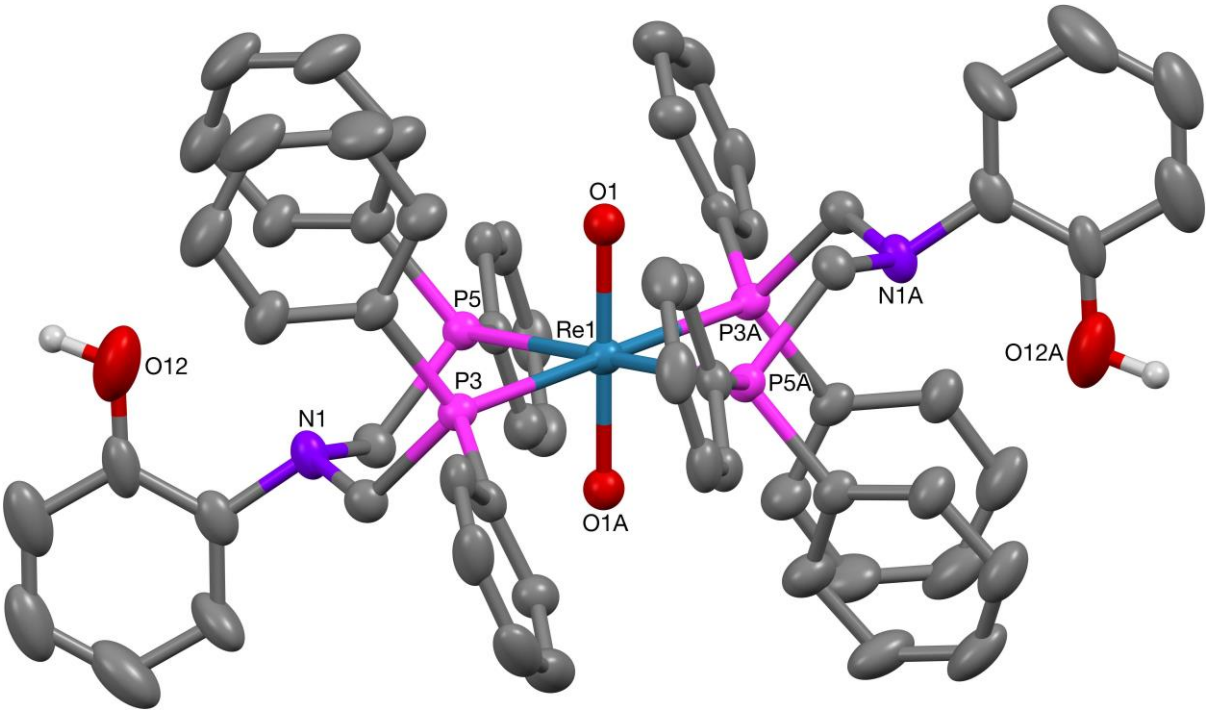

Figure S57: The structure of the *Ci*-symmetric cation present in the crystal of **Re-1** (50% probability ellipsoids).

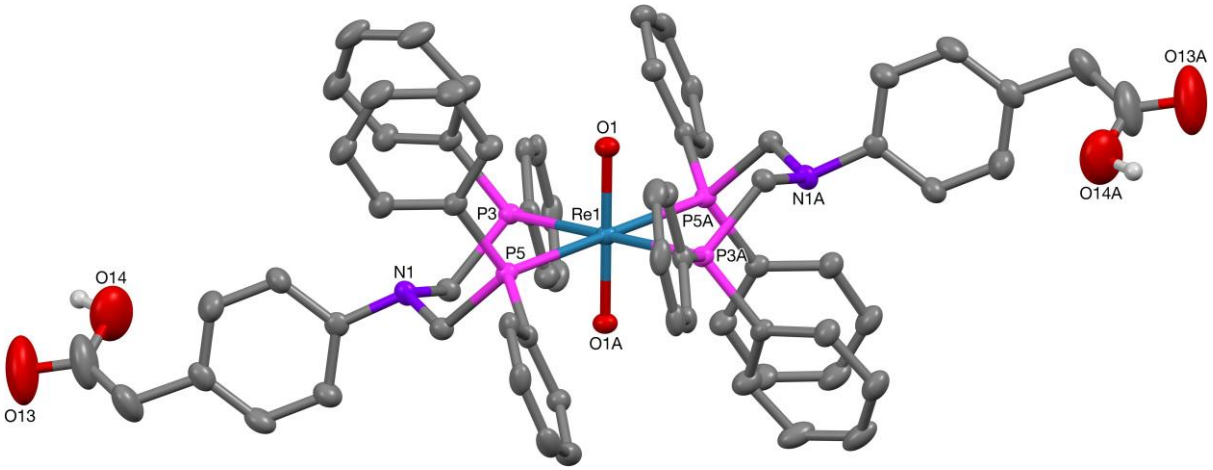

Figure S58: The structure of the *Ci*-symmetric cation present in the crystal of **Re-3** (30% probability ellipsoids).

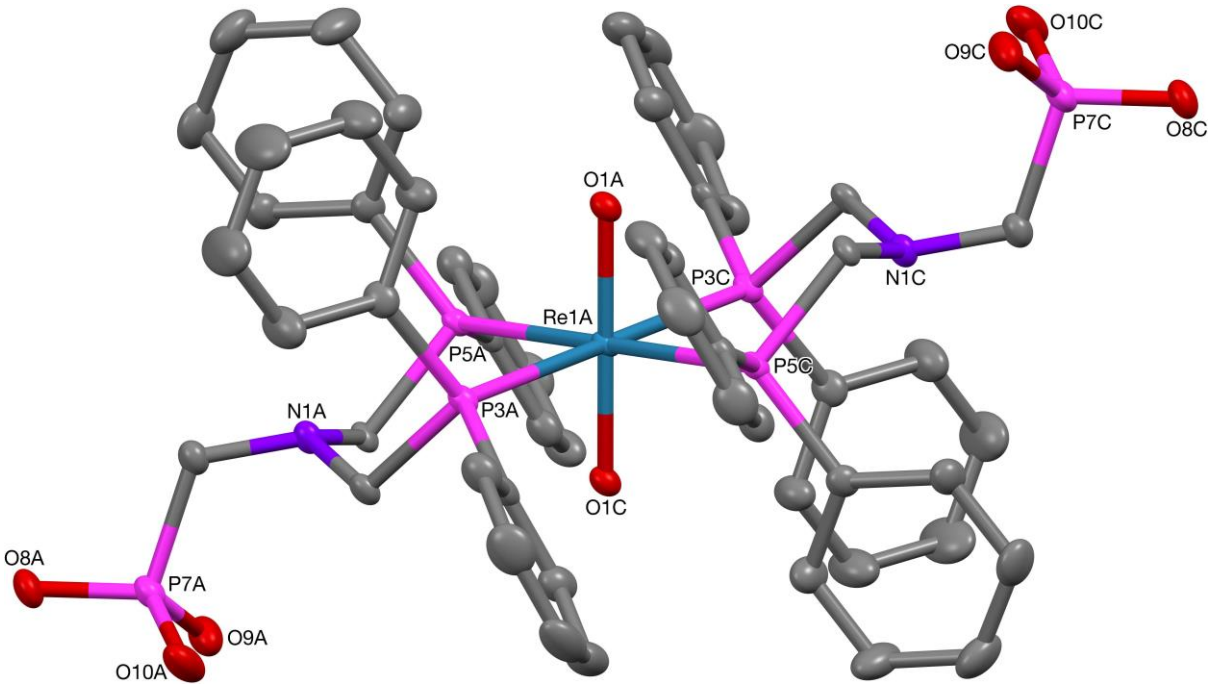

Figure S59: The structure of **Re-4-A**, one of the two independent *Ci*-symmetric cations present in the crystal of **Re-4** (30% probability ellipsoids).

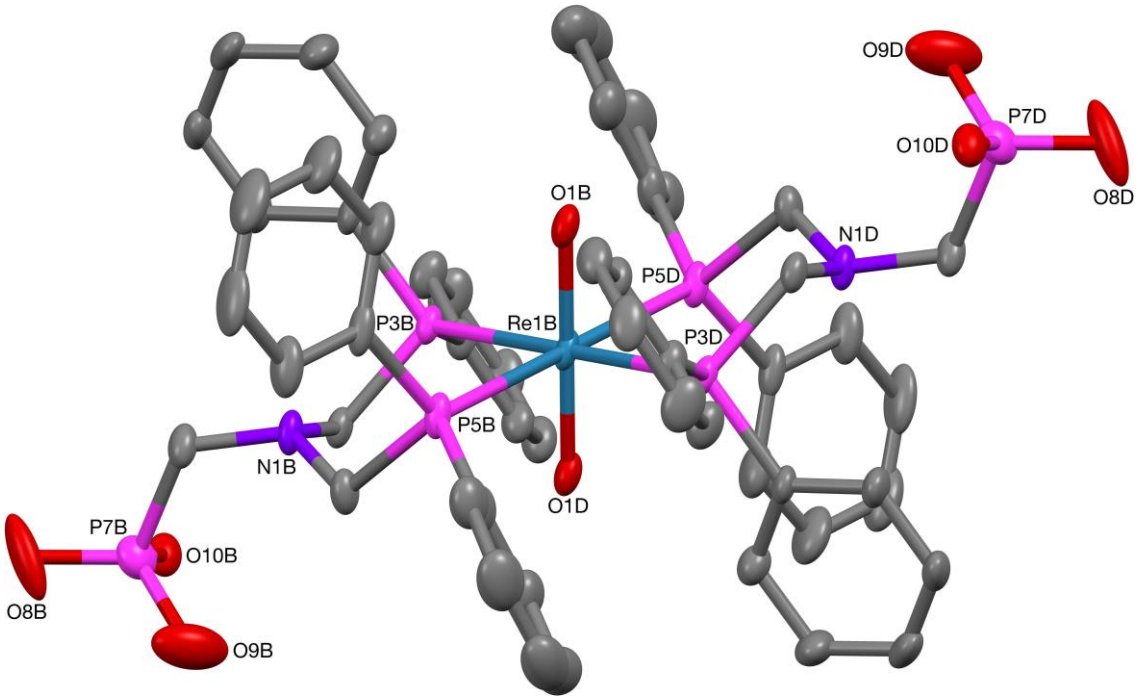

Figure S60: The structure of **Re-4-B**, one of the two independent *Ci*-symmetric cations present in the crystal of **Re-4** (30% probability ellipsoids).

S6) Biological Testing

Bacterial broth microdilution minimum inhibitory concentration (MIC) assays

Biological Assays. All compounds were obtained as dried powders and confirmed to be at > 95% purity by NMR spectroscopy and HR-MS. No further purification was performed by CO-ADD. The dry compounds were dissolved to a concentration of 10 mg mL^{-1} or 10 mM in DMSO. Samples were diluted to a final testing concentration of 32 mg mL^{-1} or 20 mM, depending on the available stock solution, while keeping the final DMSO concentration to a maximum of 0.5%, and serially diluted 1 : 2 fold for 8 times.

Antibacterial assays. For all the bacterial assays, each strain was cultured in Cation-adjusted Mueller Hinton broth (CAMHB; Bacto Laboratories 212322) at 37 °C overnight. A sample of each culture was then diluted 40-fold in fresh CAMHB and incubated at 37 °C for 1.5 – 3 h. The resultant mid-log phase cultures were diluted with CAMHB (CFU mL^{-1} measured by OD_{600}), then added to each well of the compound-containing plates (384-well non-binding surface (NBS) plates; Corning CLS3640), giving a cell density of 5×10^5 CFU mL^{-1} and a total volume of 50 mL. Plates were covered and incubated at 37 °C for 18 h without shaking. Inhibition of bacterial growth was determined measuring absorbance at 600 nm (OD_{600}), using media only as negative control and bacteria without inhibitors as positive control. MIC values were determined as the lowest concentration at which the growth was inhibited ≥ 80%. Colistin sulfate (Sigma C4461) and vancomycin HCl (Sigma 861987) were used as internal controls on each plate for Gram-negative and Gram-positive bacteria, respectively.

Antifungal assays. For the fungal assays, both fungi (yeast) strains were cultured for 3 days on Yeast Extract-Peptone Dextrose (YPD; Becton Dickinson 242720) agar at 30 °C. A yeast suspension of 1×10^6 to 5×10^6 CFU mL^{-1} (as determined by OD_{530}) was prepared from five colonies from the agar plates, and subsequently diluted with Yeast Nitrogen Base media (YNB; Becton Dickinson 233520), and added to each well of the compound-containing plates (384-well plates, NBS; Corning CLS3640) giving a final cell density of 2.5×10^3 CFU mL^{-1} and a total volume of 50 mL. Plates were covered and incubated at 35 °C for 36 h without shaking. Growth inhibition of C. albicans was determined by measuring absorbance at 630 nm (OD_{630}), while the growth inhibition of C. neoformans was determined by measuring the difference in absorbance between 600 and 570 nm ($OD_{600–570}$), after the addition of resazurin (0.001% final concentration; Sigma R7017) and incubation at 35 °C for 2 h, using media-only as negative control and fungi without inhibitors as positive control. MIC values were determined as the

lowest concentration at which the growth was inhibited at ≥ 80%. Fluconazole (Sigma F8929) was used as internal control on each plate for both strains.

Cytotoxicity assays. HEK293 ATCC CRL-1573 human embryonic kidney cells were counted manually in a Neubauer haemocytometer and added to compound-containing plates (384-well plates, tissue culture treated (TC); Corning CLS3712) giving a final density of 5000 cells per well in a and a total volume of 50 mL, using Dulbecco's Modified Eagle Medium (DMEM; Life Technologies 11995-073) with 10% Foetal Bovine Serum (FBS; GE SH30084.03). The cells were incubated together with the compounds for 20 h at 37 °C in 5% CO_2. Cytotoxicity (or cell viability) was measured by fluorescence, ex: 560/10 nm, em: 590/10 nm (F560/590), after addition of 5 mL of 25 mg mL^{-1} resazurin (2.3 mg mL^{-1} final concentration; Sigma R7017) and after further incubation for 3 h at 37 °C in 5% CO_2, using media-only as negative control and cells without inhibitors as positive control. CC_{50} (concentration at 50% cytotoxicity) were calculated by curve-fitting the inhibition values vs. log(concentration) using a sigmoidal dose–response function, with variable fitting values for bottom, top and slope. Tamoxifen (Sigma T5648) was used as internal control on each plate.

Haemolysis assays. Human whole blood (Australian Red Cross) was washed three times with 3 volumes of 0.9 % NaCl and resuspended in a concentration of 0.5 x 10^8 cells per mL, determined by manual cell count in a Neubauer haemocytometer. Washed cells were added to compound containing plates (384-well polypropylene plates (PP); Corning 3657) for a final volume of 50 mL, shaken and incubated for 1 h at 37 °C. After incubation, the plates were centrifuged at 1000 g for 10 min to pellet cells and debris, 25 mL of the supernatant was then transferred to reading plates (384 well, polystyrene plated (PS), Corning CLS3680), with haemolysis determined by measuring the supernatant absorbance at 405 mm (OD_{405}), using cells without inhibitors as negative control and cells with 1% Triton X-100 (Sigma T8787) as positive control. HC_{10} and HC_{50} (concentration at 10% and 50% haemolysis, respectively) was calculated by curve-fitting the inhibition values vs. log(concentration) using a sigmoidal dose–response function with variable-fitting values for top, bottom and slope. Melittin (Sigma M2272) was used as internal control on each plate.

Quality control. All screening is performed as two replicas (n=2), with both replicas on different assay plates, but from single plating and performed in a single screening experiment (microbial incubation). Each individual value is reported. In addition, two values are used as quality controls for individual plates: Z'-Factor=[1 - (3*(sd(NegCtrl)+sd(PosCtrl))/(average(PosCtrl)-average(NegCtrl)))] and Standard Antibiotic controls at different concentrations (>MIC and < MIC). The plate passes the quality control if Z'-Factor >0.4 and Standards are active and inactive at highest and lowest concentrations, respectively. Data not supplied.

Inhibition. Percentage growth inhibition of individual samples and concentration are calculated based on Negative Controls (media only; 100%) and Positive Controls (bacterial/cell media without inhibitors: 0%). Please note Negative inhibition values indicate that the growth rate is higher compared to the Negative Control (Bacteria/Cell only, set to 0% inhibition). The growth rates for all organisms has a variation of -/+ 10%, which lies is within expected normal distribution.

MIC (Minimum Inhibitory Concentration). The minimum inhibitory concentration (MIC) was determined following the CLSI guidelines, identifying the lowest concentration at which full inhibition of the bacteria or fungi has been detected. Full inhibition of growth has been defined at <= 20% growth (or >80% inhibition), and concentrations have only been selected if the next highest concentration displayed full inhibition (i.e. 80-100%) as well (eliminating 'singlet' active concentration). Please note MIC values are discrete values based on the concentration in a specific well.

Table S1: Primary CO-ADD screening of initial set of **Re-n** Complexes given as %-inhibition

Compound	Sa[a]	Ec[b]	Kp[c]	Pa[d]	Ab[e]	Ca[f]	Cn[g]
Re-2	95.48	-6.2	14.19	20.71	-5.76	38.45	-49.9
Re-3	98.05	5.87	31.76	8.25	0.33	17.44	71.3
Re-4	7.78	5.07	7.84	0.05	14.1	19.26	24.57
Re-5	94.52	1.61	24.36	11.67	14.31	100.4	82.15
Re-6	65.2	-5.16	11.1	-3.43	-3.56	97.76	24.57

Table S2: Dose-responsive MIC (µg/mL) CO-ADD screening of **Re-n** Complexes including CC_{50} and HC_{10} measurements

Compound	Sa[a]	Ec[b]	Kp[c]	Pa[d]	Ab[e]	Ca[f]	Cn[g]	Hk[h]	Hm[i]
Re-1	32	>32	>32	>32	>32	>32	>32	>32	4.878
Re-2	32	>32	>32	>32	>32	>32	>32	>32	>32
Re-3	16	>32	>32	>32	>32	>32	>32	27.55	>32
Re-4	-	-	-	-	-	-	-	-	-
Re-5	4	>32	>32	>32	>32	16	>32	6.724	0.952
Re-6	2	>32	>32	>32	>32	2	>32	>32	>32
Re-7	≤ 0.25	>32	>32	>32	>32	≤ 0.25	-	>32	>32
Re-8	≤ 0.25	>32	>32	>32	>32	≤ 0.25	-	>32	>32
Re-9	≤ 0.25	>32	>32	>32	>32	≤ 0.25	-	≤ 0.25	>32
Re-10	≤ 0.25	>32	>32	>32	>32	≤ 0.25	-	≤ 0.25	>32
Re-11	≤ 0.25	>32	>32	>32	>32	≤ 0.25	-	>32	>32
Re-12	≤ 0.25	>32	>32	>32	>32	≤ 0.25	-	≤ 0.25	>32
Re-13	≤ 0.25	>32	>32	>32	>32	≤ 0.25	-	≤ 0.25	>32
Re-14	≤ 0.25	>32	>32	>32	>32	8	-	>32	>32

[a]Staphylococcus aureus ATCC 43300, [b]Escherichia coli ATCC 25922, [c]Klebsiella pneumoniae ATCC 700603, [d]Acinetobacter baumannii ATCC 19606, [e]Pseudomonas aeruginosa ATCC 27853, [f]Candida albicans ATCC 90028, [g]Cryptococcus neoformans var. grubii H99; ATCC 208821, [CC5], [i]Human red blood cells.

References

1 J. Fawcett, P. A. T. Hoye, R. D. W. Kemmitt, D. J. Law and D. R. Russell, *J. Chem. Soc., Dalton Trans.*, 1993, 2563–2568.

2 S. E. Durran, M. R. J. Elsegood, N. Hawkins, M. B. Smith and S. Talib, *Tetrahedron Lett.*, 2003, **44**, 5255–5257.

3 N. Priyadarshani, B. Ginovska, J. T. Bays, J. C. Linehan and W. J. Shaw, *Dalton Trans.*, 2015, **44**, 14854–14864.

4 M. Keles, O. Altan and O. Serindag, *Heteroat. Chem.*, 2009, **20**, 232–234.

5 P. Li, R. Zaffaroni, B. De Bruin and J. N. H. Reek, *Chem. - A Eur. J.*, 2014, **21**, 4027–4038.

6 E. Bálint, E. Fazekas, G. Pinter, A. Szollosy, T. Holczbauer, M. Czugler, L. Drahos, T. Körtvélyesi and G. Keglevich, *Curr. Org. Chem.*, 2012, **16**, 547–554.

7 C. J. Weiss, A. N. Groves, M. T. Mock, W. G. Dougherty, W. S. Kassel, M. L. Helm, D. L. Dubois and R. M. Bullock, *Dalton Trans.*, 2012, **41**, 4517–4529.

8 C. Kremer, M. Rivero, E. Kremer, L. Suescun, A. W. Mombrú, R. Mariezcurrena, S. Domínguez, A. Mederos, S. Midollini and A. Castiñeiras, *Inorganica Chim. Acta*, 1999, **294**, 47–55.

9 SHELXTL v5.1, Bruker AXS, Madison, WI, 1998.

10 SHELX-2013, G.M. Sheldrick, *Acta Cryst.*, 2015, **C71**, 3-8.

11 A.L. Spek (2003, 2009) PLATON, A Multipurpose Crystallographic Tool, Utrecht University, Utrecht, The Netherlands. See also A.L. Spek, *Acta. Cryst.*, 2015, **C71**, 9-18.

Anti-microbial Resistance Collaborators,* *Lancet*, 2022, **399**, 629-655

*Christopher J L Murray, Kevin Shunji Ikuta, Fablina Sharara, Lucien Swetschinski, Gisela Robles Aguilar, Authia Gray, Chieh Han, Catherine Bisignano, Puja Rao, Eve Wool, Sarah C Johnson, Annie J Browne, Michael Give Chipeta, Frederick Fell, Sean Hackett, Georgina Haines-Woodhouse, Bahar H Kashef Hamadani, Emmanuelle A P Kumaran, Barney McManigal, Ramesh Agarwal, Samuel Akech, Samuel Albertson, John Amuasi, Jason Andrews, Aleskandr Aravkin, Elizabeth Ashley, Freddie Bailey, Stephen Baker, Buddha Basnyat, Adrie Bekker, Rose Bender, Adhisivam Bethou, Julia Bielicki, Suppawat Boonkasidecha, James Bukosia, Cristina Carvalheiro, Carlos Castañeda-Orjuela, Vilada Chansamouth, Suman Chaurasia, Sara Chiurchiù, Fazle Chowdhury, Aislinn J Cook, Ben Cooper, Tim R Cressey, Elia Criollo-Mora, Matthew Cunningham, Saffiatou Darboe, Nicholas P J Day, Maia De Luca, Klara Dokova, Angela Dramowski, Susanna J Dunachie, Tim

Eckmanns, Daniel Eibach, Amir Emami, Nicholas Feasey, Natasha Fisher-Pearson, Karen Forrest, Denise Garrett, Petra Gastmeier, Ababi Zergaw Giref, Rachel Claire Greer, Vikas Gupta, Sebastian Haller, Andrea Haselbeck, Simon I Hay, Marianne Holm, Susan Hopkins, Kenneth C Iregbu, Jan Jacobs, Daniel Jarovsky, Fatemeh Javanmardi, Meera Khorana, Niranjan Kissoon, Elsa Kobeissi, Tomislav Kostyanev, Fiorella Krapp, Ralf Krumkamp, Ajay Kumar, Hmwe H Kyu, Cherry Lim, Direk Limmathurotsakul, Michael James Loftus, Miles Lunn, Jianing Ma, Neema Mturi, Tatiana Munera-Huertas, Patrick Musicha, Marisa Marcia Mussi-Pinhata, Tomoka Nakamura, Ruchi Nanavati, Sushma Nangia, Paul Newton, Chanpheaktra Ngoun, Amanda Novotney, Davis Nwakanma, Christina W Obiero, Antonio Olivas-Martinez, Piero Olliaro, Ednah Ooko, Edgar Ortiz-Brizuela, Anton Yariv Peleg, Carlo Perrone, Nishad Plakkal, Alfredo Ponce-de-Leon, Mathieu Raad, Tanusha Ramdin, Amy Riddell, Tamalee Roberts, Julie Victoria Robotham, Anna Roca, Kristina E Rudd, Neal Russell, Jesse Schnall, John Anthony Gerard Scott, Madhusudhan Shivamallappa, Jose Sifuentes-Osornio, Nicolas Steenkeste, Andrew James Stewardson, Temenuga Stoeva, Nidanuch Tasak, Areerat Thaiprakong, Guy Thwaites, Claudia Turner, Paul Turner, H Rogier van Doorn, Sithembiso Velaphi, Avina Vongpradith, Huong Vu, Timothy Walsh, Seymour Waner, Tri Wangrangsimakul, Teresa Wozniak, Peng Zheng, Benn Sartorius, Alan D Lopez, Andy Stergachis, Catrin Moore*, Christiane Dolecek*, Mohsen Naghavi. *Contributed equally.